

**Study of a New Air Intake System for a Single Cylinder, Fuel Injection, 4 stroke  
Go-Kart engine**

by

**Safwan Hanis Bin Mohd Murad**

Dissertation submitted in partial fulfillment of  
the requirements for the  
Bachelor of Engineering (Hons)  
(Mechanical Engineering)

JANUARY 2009

Universiti Teknologi PETRONAS  
Bandar Seri Iskandar  
31750 Tronoh  
Perak Darul Ridzuan

# CERTIFICATION OF APPROVAL

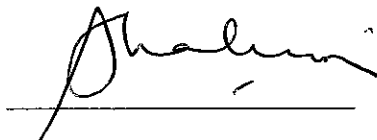
**Study of a New Air Intake System for a Single Cylinder, Fuel Injection, 4 stroke  
Go-Kart engine**

by

Safwan Hanis Bin Mohd Murad

A project dissertation submitted to the  
Mechanical Engineering Programme  
Universiti Teknologi PETRONAS  
in partial fulfillment of the requirement for the  
BACHELOR OF ENGINEERING (Hons)  
(MECHANICAL ENGINEERING)

Approved by,



(Dr. Shaharin Anwar B Sulaiman)

UNIVERSITI TEKNOLOGI PETRONAS

TRONOH, PERAK

January 2009

## CERTIFICATION OF ORIGINALITY

This is to certify that I am responsible for the work submitted in this project, that the original work is my own except as specified in the references and acknowledgements, and that the original work contained herein have not been undertaken or done by unspecified sources or persons.



---

SAFWAN HANIS BIN MOHD MURAD

## **ABSTRACT**

This report basically discusses the research done on target of designing a new air intake manifold for a Go-Kart engine. Currently the engine has difficulty in controlling fuel consumption and also emission. The objective of the research is to study a proper new air intake manifold for the conversion of a 200cc single cylinder engine from carburetor to electronic fuel injection. The study concentrates on flow characteristics in the new design of an air intake manifold that can house the electronic fuel injector as well as achieving a considerable output performance. In the content, there is the specification of the K200 engine. The report also tells on the background study conducted on obtaining enough information on the engine's behavior. A study was done on the influence of the intake manifold geometry on the performance of engine at wide range of RPM. The study was mainly to see the characteristics of air flow to the combustion chamber through an intake manifold. The study involves modeling a real combustion chamber using CATIA V5, 3D meshing and Computational Fluid Dynamics (CFD) modeling. To further strengthen the study, a flow bench experiment was conducted to validate the same condition as in the CFD. The desired results from both tests are the mass flow rate of air at specific point of the air path. Based on the preliminary results, the author proposed a design which utilizes a bell mouth and diffuser shape intake manifold design. The results of the CFD for the new design showed an increase in the mass flow rate of air entering the combustion chamber.

## **ACKNOWLEDGEMENTS**

The author wishes to take the opportunity to express his utmost gratitude to the individual and parties that have contributed their time and efforts in assisting the author in completing the project. Without their help and cooperation, no doubt the author would face some difficulties through out the project. A high appreciation to the author's supervisor, Ir Dr Shaharin Anwar B Sulaiman for his lot of guidance throughout the project. This project would not have been possible unless without his guidance and patience, the author will not succeed to complete. The author would like to thank the final year project coordinator, Prof. Vijay for his effort in ensuring the project progressed smoothly within the given time frame.

The author would like to express his utmost gratitude to the engineers at Powertrain Technology PETRONAS Research Sdn.Bhd for their trust in the author and providing the opportunity to acquire the knowledge and expertise in order to contribute to the engine development programme. The author felt very honoured to be part of the team through out the project period.

Above all, the author would like to thank his parents, who stood beside him and encouraged him constantly. A very huge appreciation to the author's brothers and sister, Syafiq, Suhail, Fatin, and especially Aimi Izzaty binti Zolkepli for being his best friend and for their continuous support and interest in what the author do. Finally, it is with the consent of the Al-mighty that everything happens as it is.

## TABLE OF CONTENTS

<b>CERTIFICATION OF ORIGINALITY</b>		iii
<b>ABSTRACT</b>		iv
<b>ACKNOWLEDGEMENT</b>		v
<b>CHAPTER 1:</b>	<b>INTRODUCTION</b>	1
	1.1 Background of Study	1
	1.2 Problem Statement	2
	1.3 Objectives	3
	1.4 Scope of Work	3
<b>CHAPTER 2:</b>	<b>LITERATURE REVIEW.</b>	4
	2.1 An Overview of Go-Kart Engines	4
	2.2 K200 Engine Specification	5
	2.3 Air Intake Manifold	7
	2.3.1 Effects of Air Intake Manifold Dimensions on Volumetric Efficiency	8
	2.3.1.1 Plenum Volume Variation	8
	2.3.1.2 Primary Pipe Length Variation	9
	2.3.1.3 Secondary Pipe Length Variation	10
	2.3.2 Fuel Induction	11
	2.3.3 Closure of the Intake Valve after BDC	11
	2.3.4 Fluid Motion into Combustion Chamber	12
	2.3.4.1 Swirl	12
	2.3.4.2 Squish and Tumble	13
<b>CHAPTER 3:</b>	<b>METHODOLOGY</b>	15
	3.1 Flow Chart	15
	3.2 Three Dimensional Modelling design in CATIA V5	17
	3.3 Meshing in GAMBIT	18
	3.4 Computational Fluid Dynamics (CFD) in FLUENT	19
	3.5 Intake Manifold Length Variation Simulation	20
	3.5.1 Boundary Conditions	21
	3.5.2 Post-Processing & Results	23
	3.5.3 Results Validation	24
<b>CHAPTER 4:</b>	<b>FLOWBENCH TEST</b>	25
	4.1 Flowbench Equipment specification	25
	4.2 Test Setup and Procedures	26
	4.2.1 Setup Procedures	27

4.2.2	Test Procedures	. . .	27
4.3	Result & Discussion	. . .	30
4.3.1	Regime 'A' (0-3mm)	. . .	30
4.3.2	Regime 'B' (3-6mm)	. . .	31
4.3.3	Regime 'C' (6-8.2)	. . .	31
4.3.4	Discussion	. . .	31
<b>CHAPTER 5:</b>	<b>CFD RESULTS AND VALIDATION</b>	. . .	32
5.1	Flow Coefficient Calculation Method		32
5.2	Example calculations of test without intake manifold at maximum valve opening	.	33
5.3	Test Data Validation	. . .	38
5.3.1	Without Intake Manifold	. . .	38
5.3.2	With Intake Manifold (204mm)	. . .	39
5.4	Discussion of Validation	. . .	40
5.5	Calculation of Entrance Region to the pipe	. . .	41
<b>CHAPTER 6:</b>	<b>PROTOTYPE DESIGN</b>	. . .	43
6.1	Diffuser to Nozzle Shape	. . .	44
6.2	Bellmouth Shape	. . .	44
<b>CHAPTER 7:</b>	<b>CONCLUSION AND RECOMMENDATIONS</b>		46
<b>REFERENCES</b>	. . . . .		48
<b>APPENDICES</b>	. . . . .		49
Appendix A:	Applied Boundary Conditions for CFD simulation	. . .	49
Appendix B:	CFD Velocity Plot of New Intake Manifold Design Analysis	. . .	50
Appendix C:	CFD Pressure Plot of New Intake Manifold Design Analysis	. . .	51
Appendix D:	Particle Tracking from CFD Simulation	. . .	52
Appendix E:	Tumble pattern from 3D simulation of 200mm length variation	. . .	53
Appendix F:	Tumble pattern from 3D simulation of 210mm length variation	. . .	54
Appendix G:	Tumble pattern from 3D simulation of 220mm length variation	. . .	55
Appendix H:	Tumble pattern from 3D simulation of 230mm length variation	. . .	56
Appendix I:	Swirl pattern from 3D simulation of 200mm length variation	. . .	57

Appendix J: Swirl pattern from 3D simulation of 210mm length variation .	58
Appendix K: Swirl pattern from 3D simulation of 220mm length variation .	59
Appendix L: Swirl pattern from 3D simulation of 230mm length variation .	60

## **LIST OF FIGURES**

Figure 1.1(a): Intake Manifold .....	2
Figure 1.1(b): Complete Assembly of K200 engine.....	2
Figure 2.1: Go-Kart under braking and low speed turn.....	4
Figure 2.2: Basic Dimension of K200 Engine.....	5
Figure 2.3: Torque Curve and Power Curve of K200 engine.....	6
Figure 2.4: Intake valve lift cam profile for K200 .....	7
Figure 2.5: Variation in volumetric efficiency with engine speed for different plenum volumes of intake manifold.....	9
Figure 2.6: Variation in volumetric efficiency with engine speed for different primary pipe length of intake manifold .....	9
Figure 2.7: Variation in volumetric efficiency with engine speed for different secondary pipe length of intake manifold .....	10
Figure 2.8: The swirling motion of flow in the combustion chamber of an engine .....	12
Figure 2.9: Tumble flow circulates around an axis perpendicular to the cylinder axis, orthogonal to swirl flow. (Pulkrabek, W. W. 2004).....	14
Figure 3.1: Flow chart of developing the new air intake manifold .....	15
Figure 3.2: Project overview and timeline for the first semester.....	16
Figure 3.3: Project overview and timeline for the second semester.....	16
Figure 3.4: Transparent 3D model of the K200 engine combustion chamber .....	17
Figure 3.5: Dimension of the K200 combustion chamber model.....	18
Figure 3.6: Meshed 3D model .....	18
Figure 3.7: Length Variation of Intake Manifold .....	21
Figure 4.1: Super Flow SF-1020 Probench .....	25
Figure 4.2: Engine cylinder head and mock intake manifold setup .....	26

Figure 4.3: Schematic drawing of cylinder head setup on flow bench.....	27
Figure 4.4: Schematic of Flow Bench Test .....	28
Figure 4.5: Schematic of Variation of Mock Intake Manifold Tested .....	29
Figure 4.6: Graph of Flowbench Test Result With Various Intake Manifold Design ...	30
Figure 5.1: Graph of Flow Coefficient Comparison of Engine without Intake Manifold between CFD and Experimental Data.....	38
Figure 5.2: Graph of Flow Coefficient Comparison of Engine with 204 mm Intake Pipe between CFD and Experimental Data.....	39
Figure 5.3: Velocity profile prediction of engine intake manifold.....	42
Figure 6.1: Isometric View of Air Intake Path of the New Proposed Design .....	43
Figure 6.2: Dimension of the side cross sectional area of the intake manifold.....	44
Figure 6.3: Graph comparison of flow coefficient Vs Valve Lift/Diameter .....	45

## LIST OF TABLES

Table 2.1: Specification of the PETRONAS K200 Engine.....	6
Table 3.1: Parameters for the mesh .....	19
Table 3.2: CFD Parameters .....	20
Table 3.3: Boundary Condition Applied for CFD Simulation.....	22
Table 3.4: FLUENT Processing parameters.....	23
Table 4.1: Flow bench SUPERFLOW equipment data acquisition accuracy.....	25
Table 4.2: Test Condition and Engine Specification.....	26
Table 5.1: Experiment 1 Engine without Intake Manifold.....	35
Table 5.2: Experiment 2 Engine Assembly with 204mm Intake Pipe.....	35
Table 5.3: Experiment 3 Engine Assembly with 102mm Intake Pipe.....	36
Table 5.4: Experiment 4 Engine Assembly with 102mm Intake pipe and a Surge Tank.....	36
Table 5.5: Experiment 5 Engine Assembly with 102mm Intake Pipe and a Surge Tank (Pipe at Upstream).....	37
Table 5.6: Experiment 6 Engine Assembly with only a Surge Tank .....	37

# CHAPTER 1

## INTRODUCTION

### 1.1 Background of Study

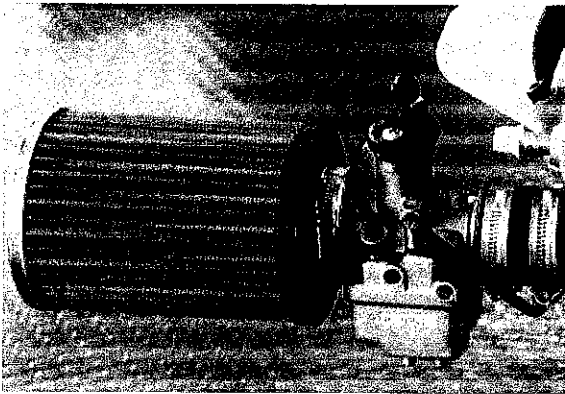
Intake manifolds have a major effect on engine performance and emission of noise and pollutants. If the air fuel ratio is maintained constant the potential for energy to release in the combustion process, is related to the quantity of air entering the cylinders. Majority of engines used in automobile applications are naturally aspirated and operate on the four-stroke cycle, in which distinct strokes are of pistons are used to induce the air and exhaust it (Cengel & Boles, 2006). These strokes enable the engine to pump gas through itself. They can be significantly affected by the design of the intake and exhaust system. Different vehicles have different engine output and applications. Each of this application requires different characteristics from the engine and a different layout of the intake manifold and exhaust manifold.

The requirement for lower noise and pollutant emission levels has further increased the importance of the design of the intake manifolds. A large proportion of the total noise generated by vehicle and stationary engines is due to the pressure waves that propagate from the intake manifold. The geometry of the manifolds has an effect on the frequency and amplitude of the waves issuing from them as noise (Winterbone & Pearson, 1999). The challenge is to obtain the desired radiated noise spectrum without producing deleterious effects on the management of the waves which enhance the engine performance.

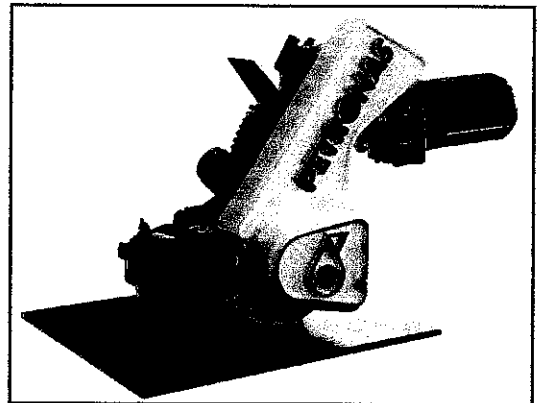
The unsteady flow in engine manifolds also has a large impact on emission levels. It is essential to understand and be able to predict the effect of the unsteady flow in the manifolds of internal combustion engines if their performance and efficiency are to be maximized while simultaneously minimizing pollutant and nose emissions.

## 1.2 Problem Statement

PETRONAS has previously developed a new single cylinder engine, 200cc, 4 stroke, petrol engine called the KELICAP 200 also known as K200 as shown in Figure 1.1(a) and (b). The engine was designed, analyzed and fabricated in Switzerland few years back. The K200 engine was designed for Go-Kart for operation with carburetor. With the current setup, very minimal engine tuning could be done. The engine consumed a lot of fuel and the emission was difficult to control. In a further development, the engine will be incorporated with an electronic fuel injection system, which will enable the control and monitoring of the amount of fuel entering the cylinder. The fuel, which will be injected into the combustion chamber can be varied throughout the entire engine RPM. Nevertheless, in order to use the new system, the engine must use an intake manifold that can house the injector together. The engine must also have an intake manifold that can facilitate the atomization process of the air and fuel efficiently into the combustion chamber. Other than that, the new air intake manifold will be designed to increase the performance of the engine through improved volumetric efficiency.



(a)



(b)

Figure 1.1 The K200 engine: (a): Intake Manifold, (b): Complete Assembly of the engine

### **1.3 Objectives**

In order to accommodate for the conversion, a new air intake manifold needs to be designed in order to mount the electronic fuel injector. The target is to increase the volumetric efficiency of air in the manifold during engine running at various RPM. The project aims to study on how to increase the volumetric efficiency of the air intake manifold of the Go-Kart engine. The design of a new intake manifold to house the electronic fuel injector is also studied.

### **1.4 Scope of Work**

In meeting the objectives of the present research, there are stages of work, which involve design, simulation, and testing. The study is within the fundamentals of a 4-stroke engine and also fluid mechanics in a pipe. The design of the inlet manifold uses a 3D modeling software. The model is meshed in software, followed by CFD simulation. From the CFD results, significant parameters such as the velocity of air flowing into the combustion chamber, mass flow rate and also the swirl and tumble ratio are analyzed for consideration in finalizing the design. Once the design is completed, the fabrication of the prototype of the intake manifold takes place to simulate the real air flow. Following to that, testings are done using the Flowbench machine to validate the parameters obtained from the CFD simulation.

## CHAPTER 2

### LITERATURE REVIEW

#### 2.1 An Overview of Go-Kart Engines

Kart racing or karting is a variant of open-wheel motor sport with simple, small four-wheeled vehicles called karts or Go-karts depending on the design. They are usually raced on scaled-down circuits. Karting is commonly perceived as the stepping stone to the higher and more expensive ranks of motorsports.



Figure 2.1: Go-Kart under braking and low speed turn

In a Go-Kart race, normally the format is a sprint race. Sprint racing takes place on dedicated kart circuits resembling small road courses, with left and right turns. Tracks go from 1/4 mile (400 m) to over 1 mile (1,600 meters) in length (James, 2004). In overall during the sprint, the engine is ramped at various RPM because of the twisty track course as shown in Figure 2.1. It is very seldom that an engine could go on a high speed for a long time. The Go-Kart needs to brake to take corners and reaccelerate again after that. What is important here is that the engine performs well by giving a high torque at even low RPM. This can be achieved with the modification to the air intake manifold. If the volumetric efficiency could be increased significantly even at low RPM, the engine output would be expected to be higher.

Racing karts use small 2-stroke or 4-stroke engines. 2-stroke kart engines are developed and built by dedicated manufacturers such as Comer, IAME (Parilla, Komet), TM, Vortex, Titan, REFO, Yamaha and ROTAX (James, 2004). These engines can develop from about 4 hp to 7 hp for a single-cylinder 60 cc unit to 90 hp for a twin 250 cc. The most popular categories worldwide are those using the Touch-and-go (TAG) 125 cc units. 100 cc 2-stroke kart engines can run in excess of 19,000 rpm while the new 125 cc KF1 engines are electronically limited at 16,000 rpm (James, 2004). Most are water-cooled today; however, previously air-cooled engines dominated the sport.

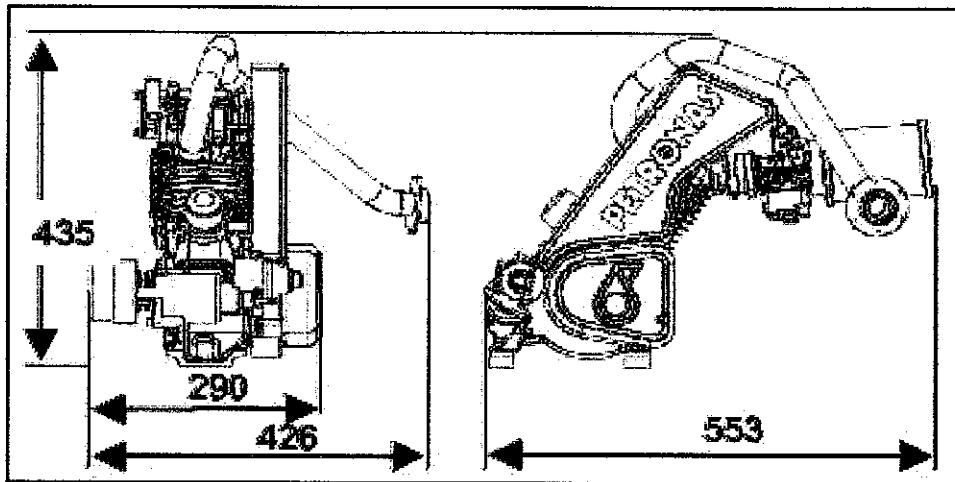


Figure 2.2: Basic Dimension of K200, Engine Powertrain Technology PETRONAS Archive, 2004

## 2.2 K200 Engine Specification

At present, the engine used by PETRONAS for Go Kart Grand Prix is a single cylinder, 4-stroke engine known as the PETRONAS K200. The dimensions are shown in Figure 2.2. Table 2.1 shows the specification of the engine (Ghazali & Ahmad, 2004). The critical parameters for the engine are the valvetrain system and also the total bore and stroke specification. There are only two valves for the cylinder, which are for the air intake and the exhaust. The challenge would be to get the best air flow rate entering single valve opening. The current torque and power output shown in Figure 2.3 will be the benchmark as the new design should at least achieve those targets considering it is already quite high compared with other single cylinder 200cc engine. The engine is also depending on an air cooled system to reduce its temperature. Therefore it is not good to keep the engine idling for a period of time, during which there is no air flow.

Table 2.1: Specification of the PETRONAS K200 Engine, Powertrain Technology  
 PETRONAS Archive, 2004

K200 specification	
Type	Single Cylinder, 4 Stroke
Displacement	199 cm <sup>3</sup>
Bore x Stroke (mm)	70 x 51.8
Valvetrain system	2 valves SOHC
Compression Ratio	10
Fuel type	Gasoline RON 95
Fuel System	Carburetor
Max. Power	13.8 kW at 9000 rpm
Max. Torque	16.5 Nm at 7000 rpm
Cooling System	Air Cooled
Lubrication System	Dry Sump
Dry Weight	14.3 kg

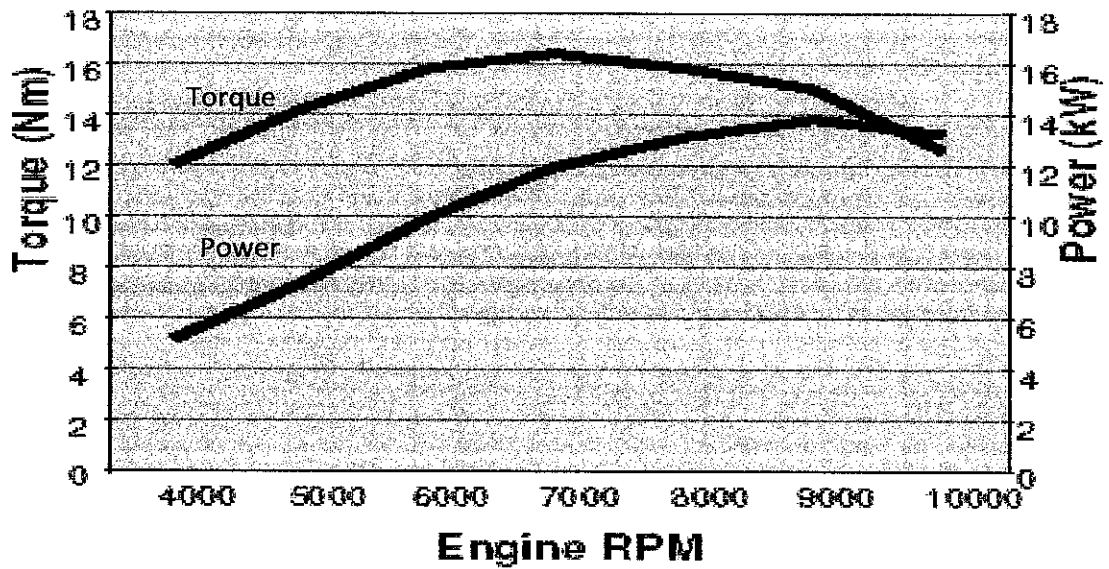


Figure 2.3: Torque Curve and Power Curve of K200 engine, Powertrain  
 Technology PETRONAS Archive, 2004

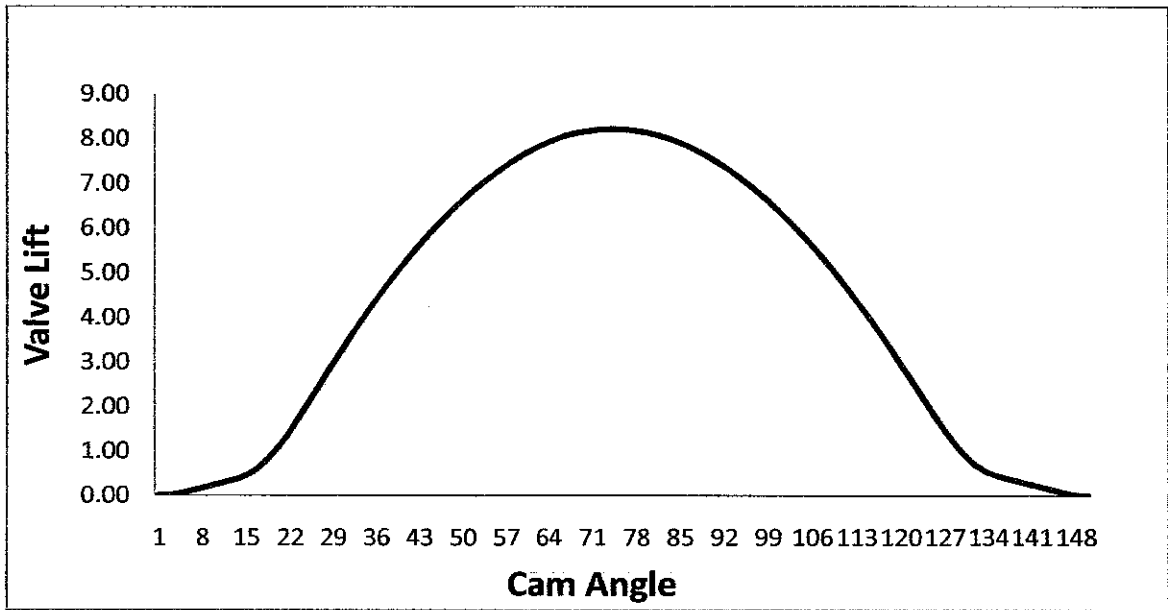


Figure 2.4: Intake valve lift cam profile for K200. POWERTRAIN TECHNOLOGY  
PETRONAS Achieve

### 2.3 Air Intake Manifold

It has long been realized that the design of inlet manifolds has a large effect on the performance of reciprocating engines. The unsteady nature of the induction means that the effect of the manifold on charging and discharging is dependable on engine speed. The inside diameter of the manifold must be large enough that a high flow resistance and the resulting low volumetric efficiency do not occur. At the same time the diameter must be small enough to assure high air velocity and turbulence, which enhances its capability of carrying fuel droplets and increases evaporation and air-fuel mixing (Winterbone & Pearson, 1999). To minimize flow resistance, runners should have no sharp bends and the interior wall surface should be smooth. This is because the impedance of the manifold is a function of the frequency of the pulses entering it (Fontana et al., 2003). The outcome of this is that it is possible to tune engine manifolds to give a particular power output characteristic as a function of speed.

In the performance of a single cylinder, the maximum output achievable from any engine is related to the amount of air that is trapped in the cylinder of the engine. This is defined by volumetric efficiency,  $\eta_v$

$$\eta_v = \frac{m_{a,t}}{m_{a,c}} \quad (2.1)$$

where  $m_{a,t}$  is mass of air trapped in cylinder and  $m_{a,c}$  is mass of air contained in swept volume of cylinder at inlet manifold density. If it is assumed that the amount of air short-circuiting through the engine cylinder is small, then it is possible to evaluate the volumetric efficiency as

$$\eta_v = \frac{60m_i}{N^*V_d\rho_i} \quad (2.2)$$

where  $m_i$  is mass flow rate of air through inlet valve,  $N^*$  equals  $N/2$  for a four-stroke engine and  $N$  for a two-stroke engine,  $N$  is engine speed (rev/min),  $V_d$  is total displacement of engine ( $m^3$ ), i.e. swept volume/cylinder x number of cylinders and  $\rho_i$  is the density of air in inlet manifold ( $kg/m^3$ )

### 2.3.1 Effects of Air Intake Manifold Dimensions on Volumetric Efficiency

In previous study on engine performance with relation to the geometry of intake manifold, (Pearson and Winterbone, 1999) did many tests to justify the engine behavior. The tests were done with single engine specification with only air intake manifold geometry that changes. The intake manifold was a modular construction so that the primary pipe length, plenum volume and secondary pipe length could be varied. Pipe diameters were not varied in the experimental exercise and it is possible that these could affect the values of the attenuation coefficients. All of the data had been taken at wide open throttle.

#### 2.3.1.1 Plenum Volume Variation

A comparison of predicted volumetric efficiency for manifolds with identical primary and secondary pipe dimensions but different plenum volumes is shown in Figure 2.5. It can be seen that increasing the plenum volume decreases the engine speed at which the lower speed peak in the volumetric efficiency curve occurs and the magnitude of the peak is also reduced. The plenum volume can have a profound effect on idle speed control and this could be beneficial although it reduces performance.

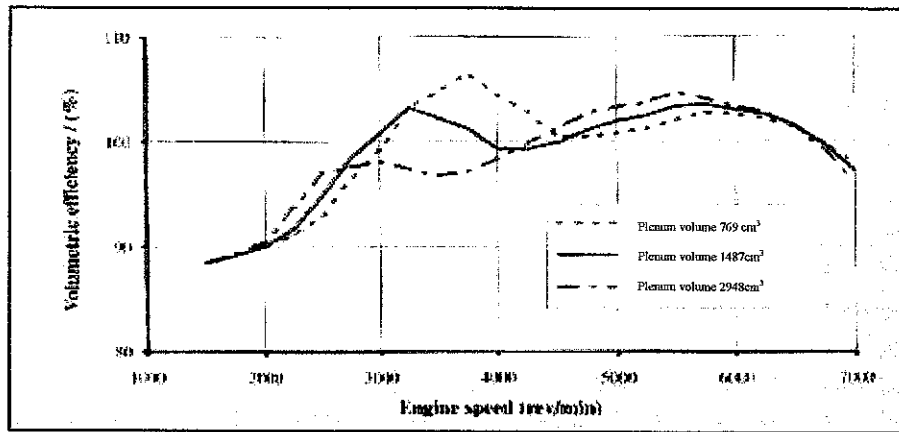


Figure 2.5: Variation in volumetric efficiency with engine speed for different plenum volumes of intake manifold (Pearson & Winterbone, 1999)

### 2.3.1.2 Primary Pipe Length Variation

In Figure 2.6 shows the resulting volumetric efficiency at which the secondary pipe length and plenum volume is kept constant throughout various RPM. From the test, lengthening the primary pipe decreases the engine speed at which the high speed volumetric efficiency peak occurs and also increases its magnitude. However, the range of which benefit is achieved is reduced.

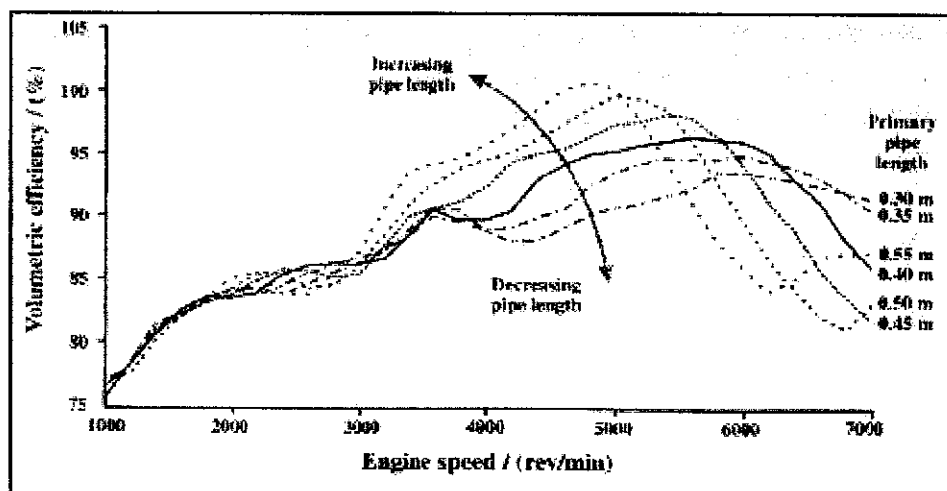


Figure 2.6: Variation in volumetric efficiency with engine speed for different primary pipe length of intake manifold (Pearson & Winterbone, 1999)

### 2.3.1.3 Secondary Pipe Length Variation

The effect of changing the manifold secondary pipe length on the volumetric efficiency curve is shown in Figure 2.7. By increasing the secondary pipe length will decrease the engine speed at which the lower speed peak occurs. The higher speed peak is largely unaffected by this modification. By varying the secondary pipe length enables the engine to maintain a high volumetric efficiency across wide range of engine RPM.

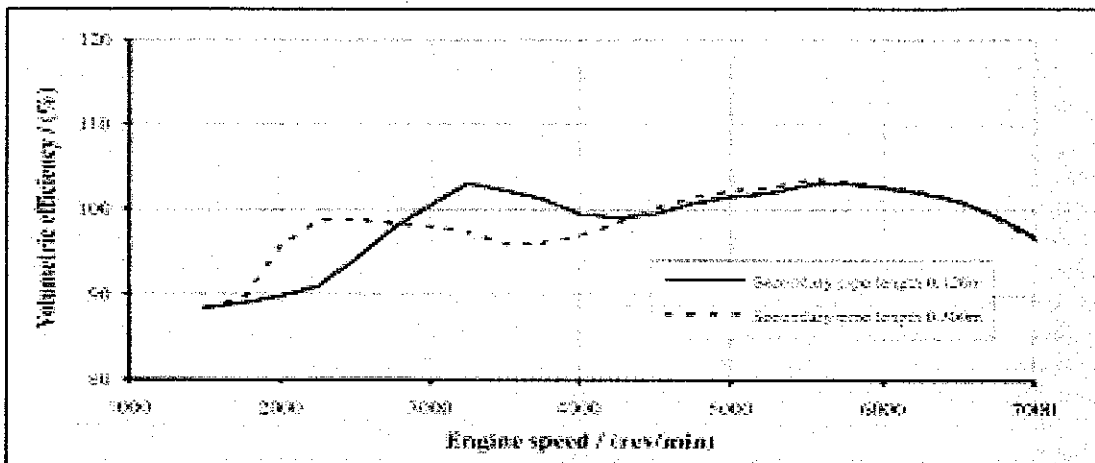


Figure 2.7: Variation in volumetric efficiency with engine speed for different secondary pipe length of intake manifold (Pearson & Winterbone, 1999)

### **2.3.2 Fuel Induction**

Fuel is added to inlet air somewhere in the intake system such as before the manifold, in the manifold and even directly into the cylinder. The further upstream the fuel spray can travel, the more time there is to evaporate its droplets and obtain proper mixing of the air and fuel vapor. However, this also reduces engine volumetric efficiency by displacement of the incoming air by the fuel vapor. Fuel vapor mixes with the air and flows with it. Very small liquid fuel droplets are carried by the airflow, smaller droplets following the streamlines better than larger droplets because with mass inertia higher than that of air, liquid particles will not always flow at the same velocity as the air and will not flow around corners readily, larger droplets deviating more than smaller ones (Pulkrabek, 2004). The third way fuel flows through the manifold is in a thin liquid film along the walls. This film occurs because gravity separates some droplets from the flow and when other droplets strike the wall where the runner executes a corner. The length of a runner to a given cylinder and the bends in it will influence the amount of fuel gets carried by a given flow rate.

### **2.3.3 Closure of the Intake Valve after BDC**

The timing of the closure of the intake valve affects the quantity of air that ends up in the cylinder. Near the end of the intake stroke, the intake valve is open and the piston is moving from TDC towards BDC (Halderman, 2005). Air is pushed into the cylinder through the open intake valve due to the vacuum created by the additional volume being displaced by the piston. There is a pressure drop in the air as it passes through the intake valve, and the pressure inside the cylinder is less than the pressure outside the cylinder in the intake manifold. The ideal time for the intake valve to close is when this pressure equalization occurs between the air inside the cylinder and air in the manifold (Pulkrabek, 2004). If it closes before this point, air that is still entering the cylinder is stopped and a loss of volumetric efficiency is experienced. If the valve is closed after this point, air being compression by the piston will force some air back out of the cylinder, again with a loss in volumetric efficiency.

### 2.3.4 Fluid Motion into Combustion Chamber

The motion of fluid into the combustion chamber is important to speed the evaporation of fuel, to enhance air-fuel mixing and to increase combustion speed and efficiency (Srinivasan, 2001). Due to the high velocities involved, all air flows within the engine system are turbulent. As a result of turbulence, the thermodynamic heat transfer rates within the engine are increased by an order of magnitude. As the engine speed increases, the flow rates increase, with a corresponding increase in swirl, squish and turbulence (McLandress et al., 2005). This increases the real time rate of fuel evaporation, mixing of the fuel vapor and air and combustion. The high turbulence near TDC when ignition occurs is very desirable for combustion. It breaks up and spreads the flame front many times faster than that of a laminar flame.

#### 2.3.4.1 Swirl

The main bulk mass motion within the cylinder is a rotational motion called swirl (Pulkrabek, 2004). It is generated by constructing the intake system to give a tangential component to the intake flow as it enters the cylinder as shown in Figure 2.8. This is done by shaping and contouring the intake manifold, valve ports and sometimes even the piston face.

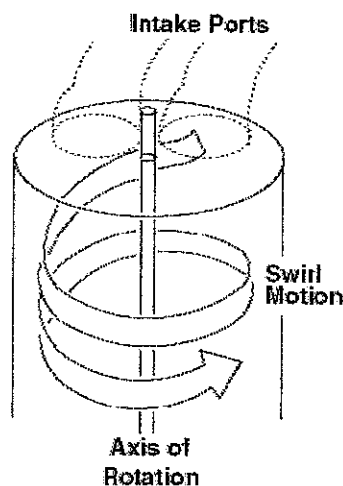


Figure 2.8: The swirling motion of flow in the combustion chamber of an engine.

(Pulkrabek, 2004)

Swirl greatly enhances the mixing of air and fuel to give a homogeneous mixture in the very short time available for the engine. (Rathnaraj, 2007) Swirl ratio is a dimensionless parameter used to quantify rotational motion in the cylinder. It is defined in two ways in the technical literature:

$$(SR)_1 = \frac{\omega}{N} \quad (2.3)$$

$$(SR)_2 = \frac{U_t}{U_p} \quad (2.4)$$

where  $\omega$  is angular speed,  $N$  is engine speed;  $U_t$  is swirl tangential speed and  $U_p$  is average piston speed. Average values of either the angular speed or the tangential speed should be used in these equations. The Swirl ratio continuously changes after BDC in the compression stroke due to viscous drag with the cylinder walls. The Maximum swirl ratio as defined in Eq (2.3) can be on the order of 5 to 10 (Laramée et al., 2004).

#### 2.3.4.2 Squish and Tumble

When the piston approaches TDC at the end of the compression stroke, the volume around the outer edges of the combustion chamber is suddenly reduced to a very small value. As the piston approaches TDC, the gas mixture occupying the volume at the outer radius of the cylinder is forced radially inward as this outer volume is reduced to near zero. The radial inward motion of the gas mixture is called squish (Pulkrabek, 2004). As the piston nears TDC, squish motion generates a secondary rotational flow called tumble as shown in Figure 2.9. This rotation occurs about a circumferential axis near the outer edge of the piston bowl. It is one of the important parameters in establishing the stratification of the air-fuel mixture in those engines which operate with the common combustion pattern. Tumble ratio is the dimensionless parameter used to characterize the magnitude of tumble (Laramée et al., 2004):

$$TR = \frac{\omega_t}{N} \quad (2.5)$$

where  $\omega_t$  is angular speed of tumble and  $N$  is engine speed.

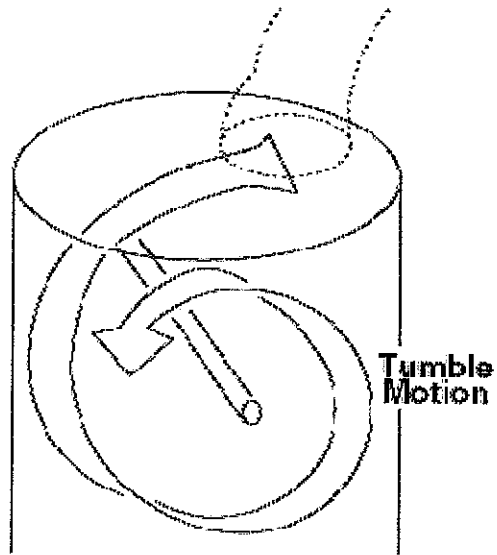


Figure 2.9: Tumble flow circulates around an axis perpendicular to the cylinder axis, orthogonal to swirl flow (Pulkrabek, 2004)

## CHAPTER 3 METHODOLOGY

### 3.1 Flow Chart

The methodology taken to do this project is shown in Figure 3.1. At the beginning, the approach is to do benchmarking studies among few similar single cylinder engines, in order to get performance comparison. After doing some benchmarking studies, a design concept can be produced based on other engines. From the design concept, engineering calculations such as fluid mechanics theories will be used to further optimize the design in 3D modeling software named CATIA V5.

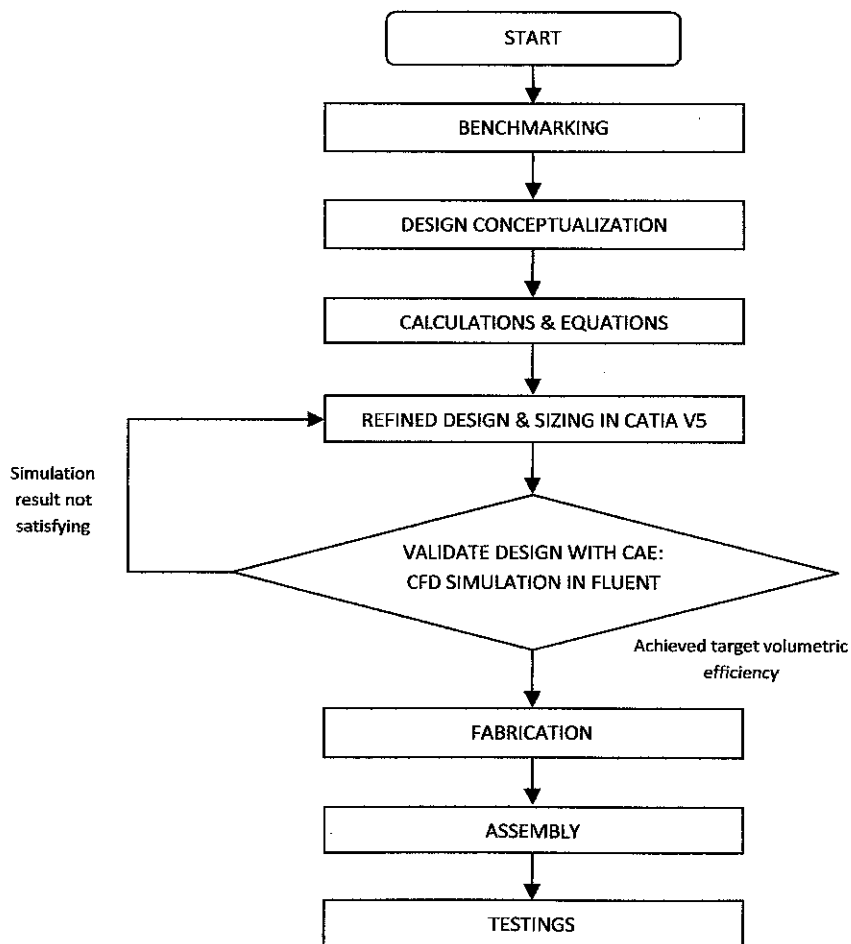


Figure 3.1: Flow chart of developing the new air intake manifold

### Project Timeline 1

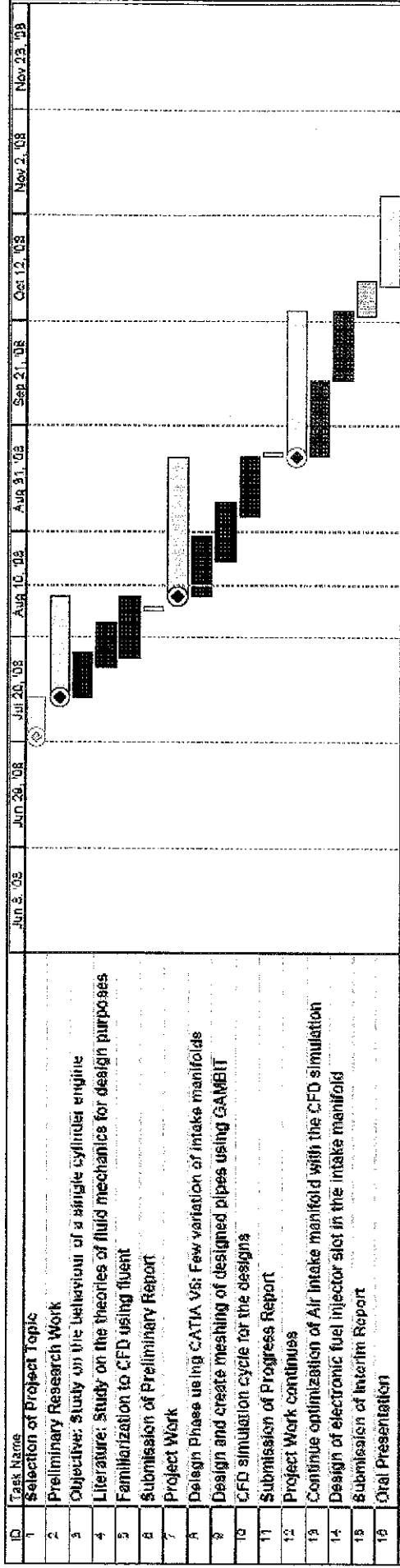


Figure 3.2: Project overview and timeline for the first semester

### Project Timeline 2

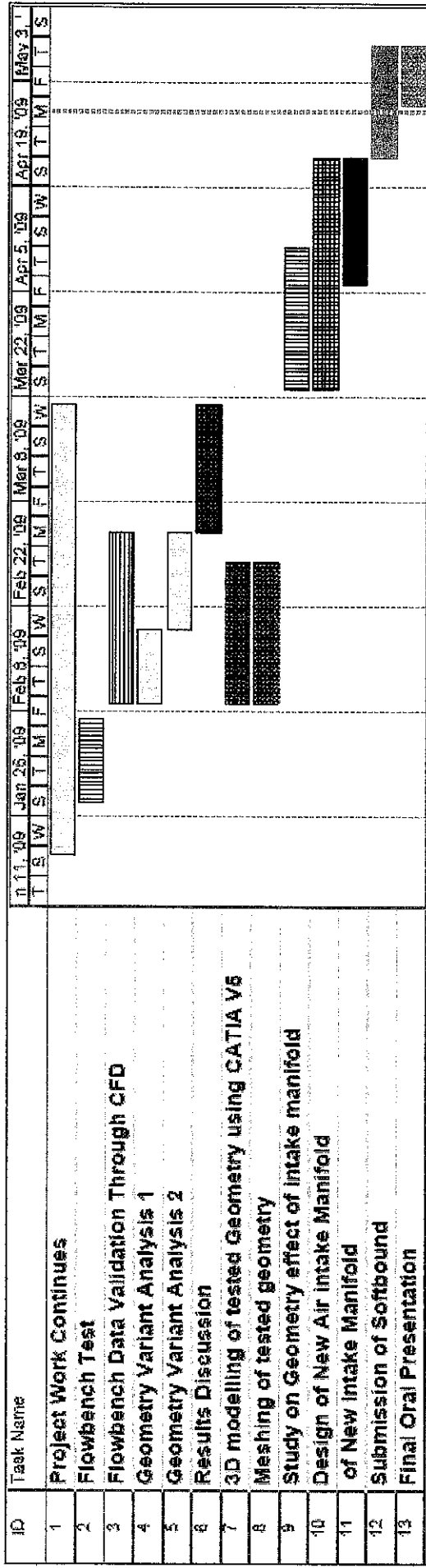


Figure 3.3: Project overview and timeline for the second semester

The important outcome from the calculation would be the sizing of the air intake manifold as to get the best volumetric efficiency of air going into the combustion chamber. The next step is to validate the design and functionality of the air intake manifold through Computational Fluid Dynamics simulation using software named FLUENT. If the design has proven its performance, the final design will go through final stage of modeling and be assembled in the CATIA itself. The details of work to be done and together with the timeline are listed in Figure 3.2 and 3.3.

### **3.2 Three Dimensional Modeling Design in CATIA V5**

In order to get accurate simulation, the design in the 3D modeling needs to resemble the exact geometry of the engine, especially components in the combustion chamber. The geometry of the intake port, intake valve and combustion chamber is taken from previous CAD file from Powertrain Technology PETRONAS. The 3D model design will resemble the path of air entering the combustion chamber. In order to export the model to be meshed and simulate later, the model has to be all solid. Only the volume of air path needs to be modeled, as the outer detail is not necessary. Figure 3.4 shows model of the combustion chamber. The model is set to have maximum valve lift of 8.2 mm and maximum cylinder volume of 199 cm<sup>3</sup> as shown in Figure 3.5.

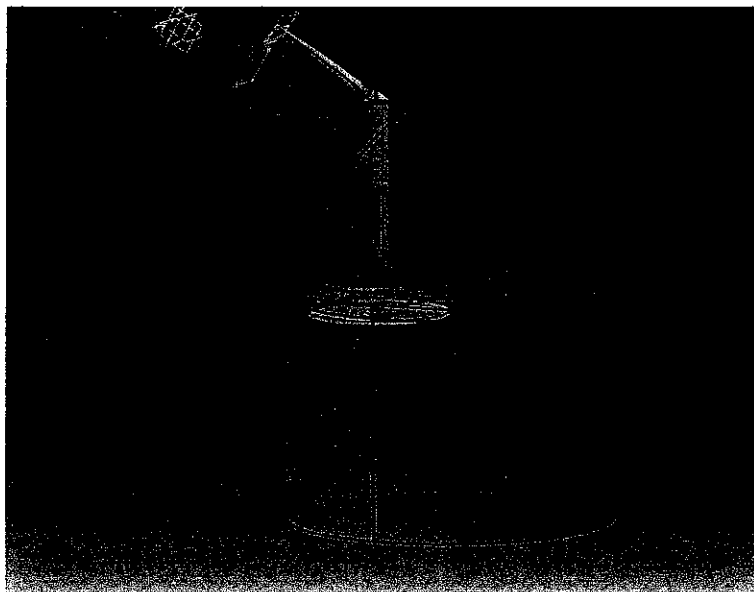


Figure 3.4: Transparent 3D model of the K200 engine combustion chamber

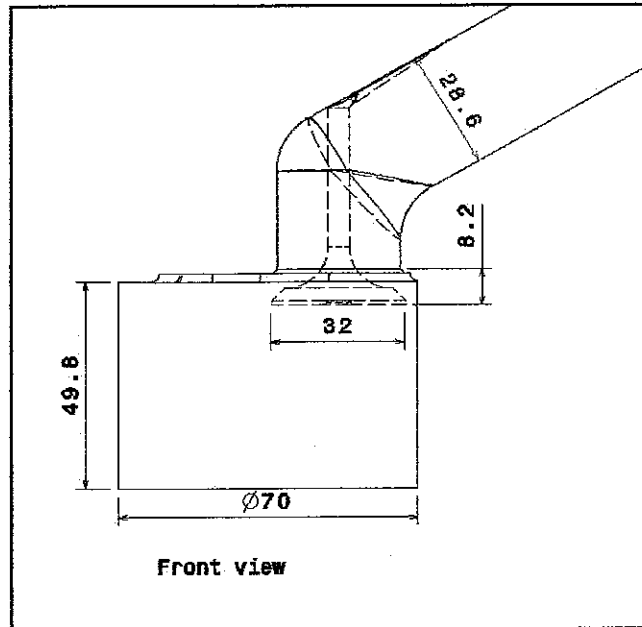


Figure 3.5: Dimension of the model for the K200 engine combustion chamber

### 3.3 Meshing in GAMBIT

When the design is done, the CATIA file will be imported to meshing software called GAMBIT. The CATIA file is converted to IGS file and exported to GAMBIT. Figure 3.6 shows the meshing component of the design.

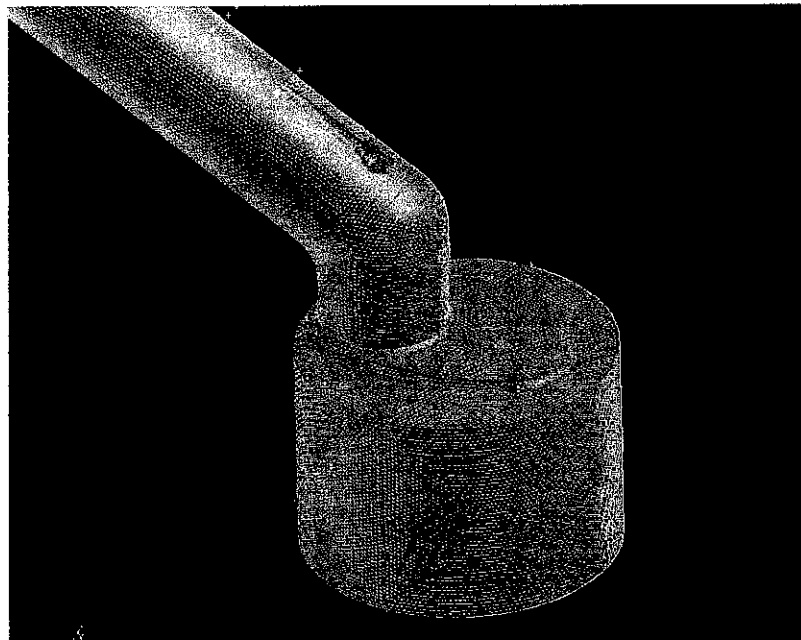


Figure 3.6: Meshed 3D model

The part is meshed to the requirement of the CFD analysis. In here, it is define the amount of spacing between meshes. The smaller the mesh interval spacing, the higher accuracy of the CFD analysis. However, there are limitations to how detail can the computer process and can the processor cope with lots of meshes. The best way is to refine at the area where results of analysis is critical for instance here is the combustion chamber. The resulting amount of mesh volume for this part is 1,437,285 with interval spacing of 1mm, which is considered very detail for a small part as this. The meshed model file is then exported to FLUENT to be analyzed using CFD. Table 3.1 shows the parameters for the CFD simulation with total amount of 10000 iterations.

Engine parameters

Table 3.1: Parameters for the mesh

Intake manifold diameter	28.3mm
Engine Bore	70mm
Engine Stroke	51.8mm
Valve Lift	8.2mm

Mesh Parameters

Mesh Type	Tetrahedral, interval spacing = 1
Meshed Cells	1,423,453

### 3.4 Computational Fluid Dynamics (CFD) in FLUENT

In here the meshed 3D model is imported to FLUENT and all the parameters are applied. These parameters need to be specified correctly in order to get accurate result. There are few parameters that are calculated by the software and some by the user first. The boundary condition for the simulation has to be determined by the user. For this, there is only one boundary condition which is the Velocity Inlet at the entrance of the intake manifold. Table 3.2 shows the CFD parameters necessary for the simulation.

Table 3.2: CFD Parameters

Viscous Model	k-epsilon (2 equation)
Time Base	Steady State
Fluid Type	Air, density: 1.225 kg/m <sup>3</sup>
Flow	Turbulent
Space Model	3D
Velocity Formulation	Absolute
Turbulence intensity	4%
Reynolds Number	23765 (Turbulent)
Targeted Number of Iterations	10,000

The parameters will be standard for all of the 3D models that will be simulated with varied geometry. This is to get similar operating conditions and the results can be compared between each model. From the comparison, we can select the best result which in this case would be the one having best mass flow rate, swirl coefficient and tumble coefficient. From there we can calculate the volumetric efficiency.

### 3.5 Intake Manifold Length Variation Simulation

A normal CFD simulation was conducted to validate the behavior of the air coming into the combustion chamber with various intake manifold lengths. The first model is fitted with a 200 mm intake manifold and the others will be an increment in length by 10 mm every time. Figure 3.7 shows the variations of the intake manifold length. The Meshing activity for every variation will be using the same interval spacing of 1mm. The CFD parameters are also same as the previous parameters shown. The target results of these simulations will be to validate the tangential velocity of the air entering and circulating the combustion chamber. With different length of intake manifold, the behavior of air will be different as the velocity of air is affected.

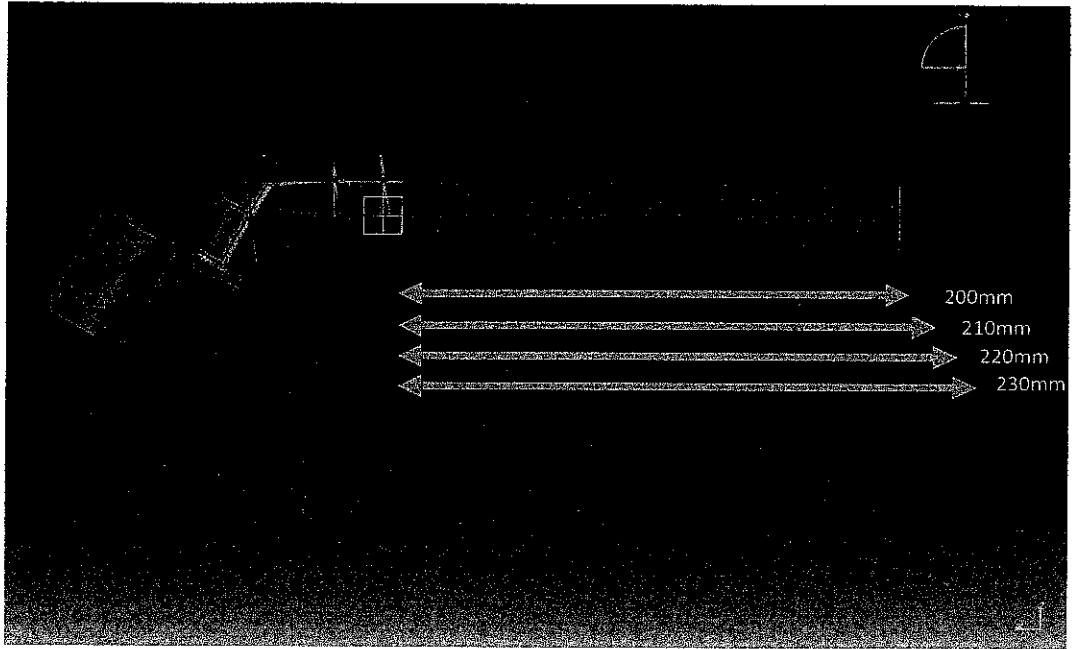


Figure 3.7: Length variation of the intake manifold

### 3.5.1 Boundary Conditions

The boundary conditions applied to the model are as shown in Appendix A. The velocity inlet at the entrance of the air intake manifold is 15 m/s. This is calculated base on the running speed of the engine.

$$v_s = \sqrt{\frac{2\gamma}{\gamma-1} RT \left[ 1 - \frac{P_2}{P_1} \right]^{\frac{\gamma-1}{\gamma}}} \quad (3.1)$$

where  $v_s$  is the isentropic flow velocity,  $\gamma$  is the air isentropic component, R is the gas constant, T is the air temperature,  $P_1$  is the air pressure at valve upstream and  $P_2$  is the air pressure at valve downstream (Nor, 2004).

The theoretical mass flow rate,  $\dot{m}_{theoretical}$  is calculated using the following equation:-

$$\dot{m}_{theoretical} = A_k \rho_s V_s \quad (3.2)$$

where  $A_k$  is the valve seat area,  $\rho_s$  is the isentropic air density.

Table 3.3: Boundary Condition Applied for CFD Simulation

<b>Boundary Condition</b>	<b>Details</b>
<b>Inlet Pressure</b>	101.325 kPa
	Backflow Specification Method: Normal to Boundary
	Turbulence Specification Method: Intensity and Hydraulic Diameter
<b>Outlet Pressure</b>	96.084 kPa (Flow bench Test Parameter)
	Backflow Specification Method: Normal to Boundary
	Turbulence Specification Method: Intensity and Hydraulic Diameter
<b>Intake Manifold Wall Roughness</b>	8 $\mu\text{m}$ (Nor, 2004)
	No Slip Condition
	Stationary Wall
<b>Cylinder Head Wall Roughness</b>	25 $\mu\text{m}$ (Nor, 2004)
	No Slip Condition
	Stationary Wall

For this CFD model, there are no energy and radiation model applied because temperature is not taken into consideration. This is because to simplify the iterations and concentrate more on the air flow into the combustion chamber. Future works may want to include this if combustion is modeled together. Table 3.3 shows the boundary conditions applied for all variations of air intake manifold design simulated.

Table 3.4 shows the CFD processing parameters. The parameters will determine the level of detail the simulation will be.

Table 3.4: FLUENT Processing parameters

<b>Solution Control</b>	<b>Details</b>
Pressure Velocity Coupling	SIMPLE
Pressure Discretization	Second Order
Momentum Discretization	Second Order Upwind
Turbulent Kinetic Energy Discretization	Second Order Upwind
Turbulent Dissipation Rate Discretization	Second Order Upwind

### 3.5.2 Post-Processing & Results

The results of the CFD simulation are shown in Appendix B. The results show the behavior of the air when entering the combustion chamber as a result of the intake manifold length variation. The Figures are sliced into two different views which are parallel to the combustion chamber plane and another is perpendicular to it. This is to view the motion of swirl and tumble of air in the combustion chamber. From the results in Appendix L, it is shown that the longest pipe seems to create a high amount of swirl compared to the other lengths.

### **3.5.3 Results Validation**

In order to validate the results of the simulation, a flowbench test has to be conducted. The flowbench can simulate the same conditions as specified in the CFD. The port flow measurement will be conducted using a sand-cast aluminium alloy cylinder head previously fabricated, with the bench rig at Powertrain Technology PETRONAS, PRSB. The Intake manifold pipe will be fabricated using stainless steel pipe welded together using TIG (Tungsten Inert Gas) welding with various lengths. The pipes will be attached to the alloy cylinder to simulate using flowbench rig. From the test, it is possible to extract data such as the flow coefficient, mass flow rate, swirl ratio and tumble ratio. The results gained can be compared to the one obtained from CFD simulation.

## CHAPTER 4

### FLOWBENCH TEST

#### 4.1 Flow bench Equipment specification

Flow bench is equipment that is used to model and measure the characteristics of air entering the intake manifold and combustion chamber. Figure 4.1 shows the flow bench used which is the Super Flow SF-1020. Table 4.1 shows the accuracy of data acquisition of the equipment.

Table 4.1: Flow bench SUPERFLOW equipment data acquisition accuracy

Flow Measurement Accuracy	$\pm 0.05\%$ of reading in normal operating ranges Repeatability: $\pm 0.25\%$ of reading Range: 0 – 1000 cfm (0-470 l/s)
Test Pressure Accuracy	$\pm 0.05"$ ( $\pm 0.13$ cm) of water
Pressure Range	0-65" (0-165 cm) of water
Temperature Measurement Accuracy	$\pm 0.5^\circ$ F ( $\pm 0.3^\circ$ C)

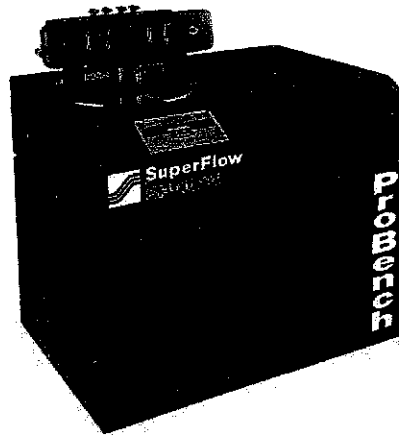


Figure 4.1: Super Flow SF-1020 Probench

## 4.2 Test Setup and Procedures

Table 4.2: Test Condition and Engine specification

Test Condition	
Pressure Difference over atmosphere:	450 mm of water column
Air Temperature	25°C (Air Conditioned Room)
Engine Specification	
Intake Valve Diameter	32 mm
Maximum Intake Valve Lift	8.2 mm
Maximum Exhaust Valve Lift	Remain closed
Cylinder Head, Valve Seat Profile	Same configuration

The experiment was conducted using the K200 engine cylinder head. Only the intake valve was controlled with a maximum opening of 8.2 mm. The air temperature was measured to determine the density of air running through the intake manifold. The pressure difference was set at about 450 mm water column to have negative pressure at the downstream of the flow bench.

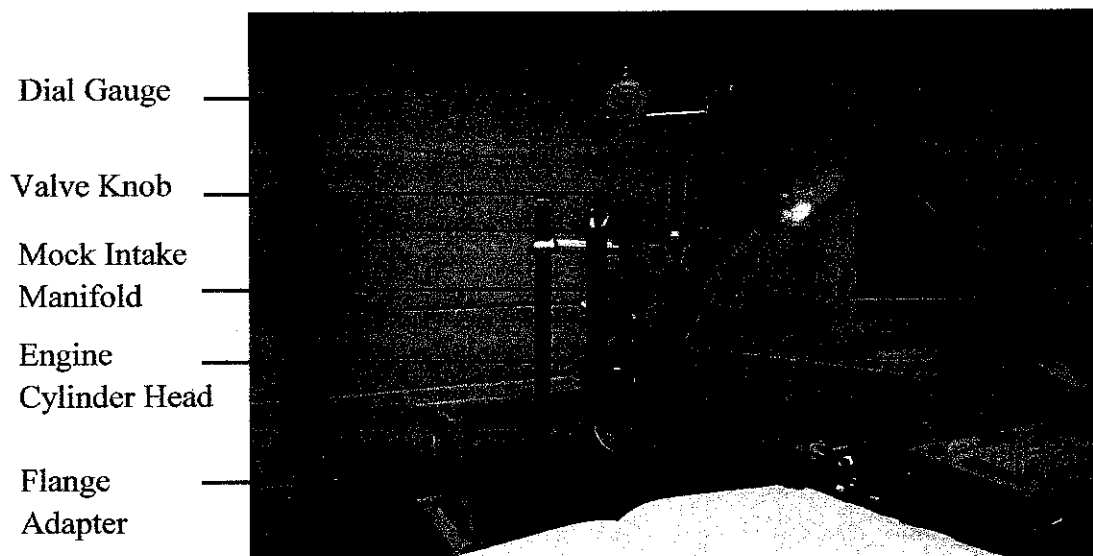


Figure 4.2: Engine cylinder head and mock intake manifold setup

#### 4.2.1 Setup Procedures

The cylinder head of the engine with complete valves assembly is used for this test as shown in Figure 4.2. The cylinder head assembly is placed on an acrylic made mock combustion chamber. Silicon glue is used to seal the cylinder head to the acrylic surface. A dial gauge is mounted at the top of the bolt used to push the intake valve down. This is to monitor the change in valve lift. Once the assembly is done, it is then placed on top of the air opening of the flow bench equipment. The mock intake manifold is then assembled to the cylinder head by using clay without interrupting the airflow to the combustion chamber.

#### 4.2.2 Test Procedures

At startup, the intake and exhaust valve will be at closed position and the machine is set to have a suction of 20-in H<sub>2</sub>O. Before adjusting the valve lift, it is important to wait till the reading of the air pressure is at almost 20-in H<sub>2</sub>O. Figure 4.3 shows the flow path of air into the flow bench equipment.

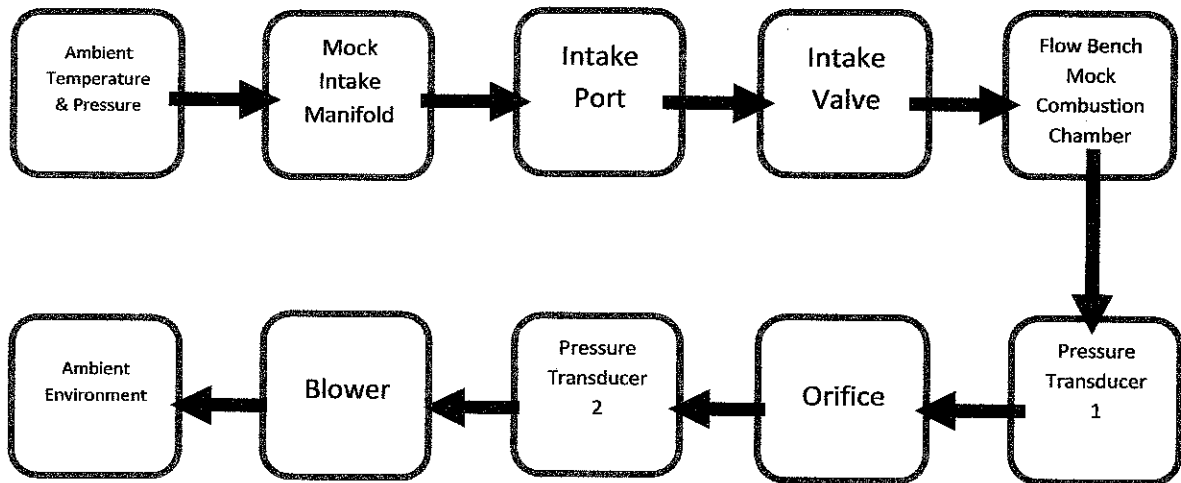


Figure 4.3: Schematic drawing of cylinder head setup on flow bench

Once the pressure reading give difference about only 0.25, the valve could be pushed down at about 1mm at a time. Data of mass flow rate in cubic feet per minute (cfm) was taken for every increment of 1mm of valve lift up till 8.2mm. The test is repeated with variations of other mock intake manifold design as shown in Figure 4.5 and data was collected.

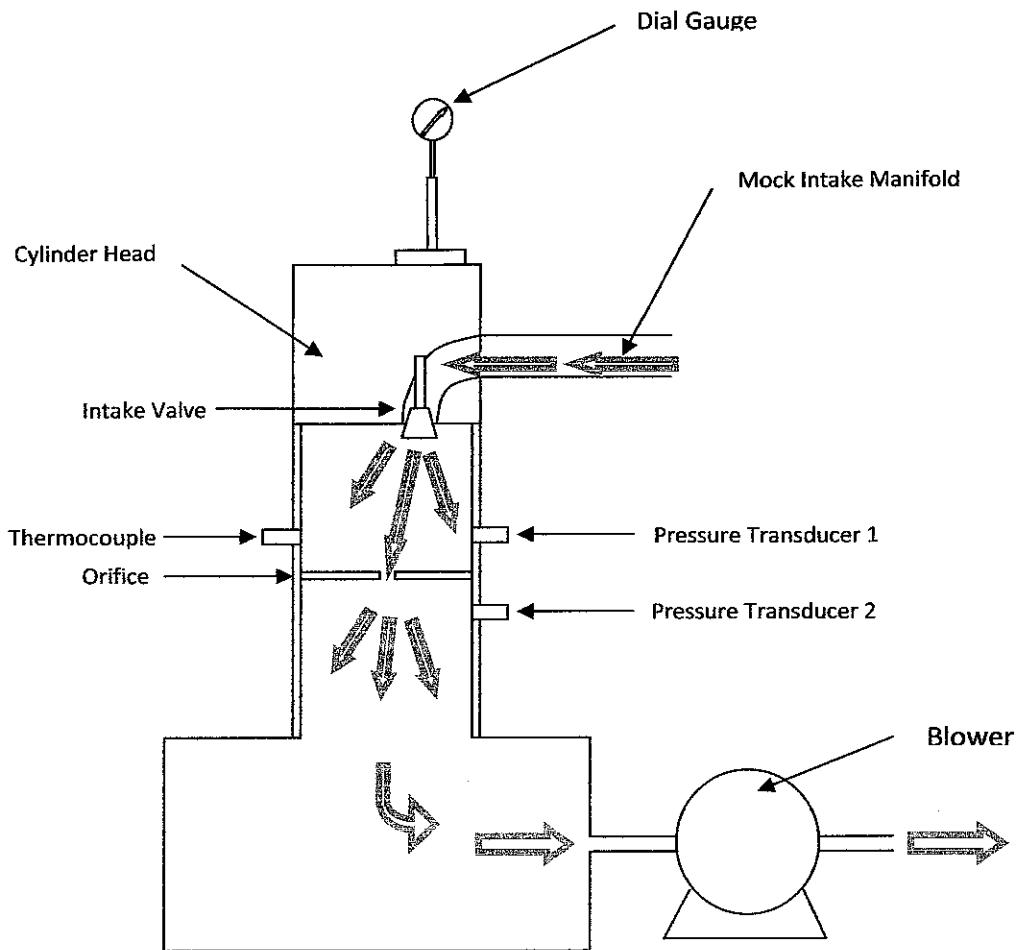


Figure 4.4: Schematic of Flow Bench Test

The flow bench test was conducted to validate the accuracy of results from CFD. In order to achieve the best results, it would be best if the conditions from the flow bench test are matched to the CFD parameters. The parameters are the geometry wise, boundary conditions. In the project, the weakness of the comparison was that the geometry of the 3D model was not exactly the same as in the flow bench. In the flow bench, there is an orifice as shown in Figure 4.4 that was used to measure the pressure difference of the downstream area.

The result of the experiment may differ if the CFD is modeled with the orifice included. The result as for now shows that the difference in mass flow rate is quite significant. For future experiment, the geometry must be modeled as close as possible to that of the experiment to make sure that the conditions are the same.

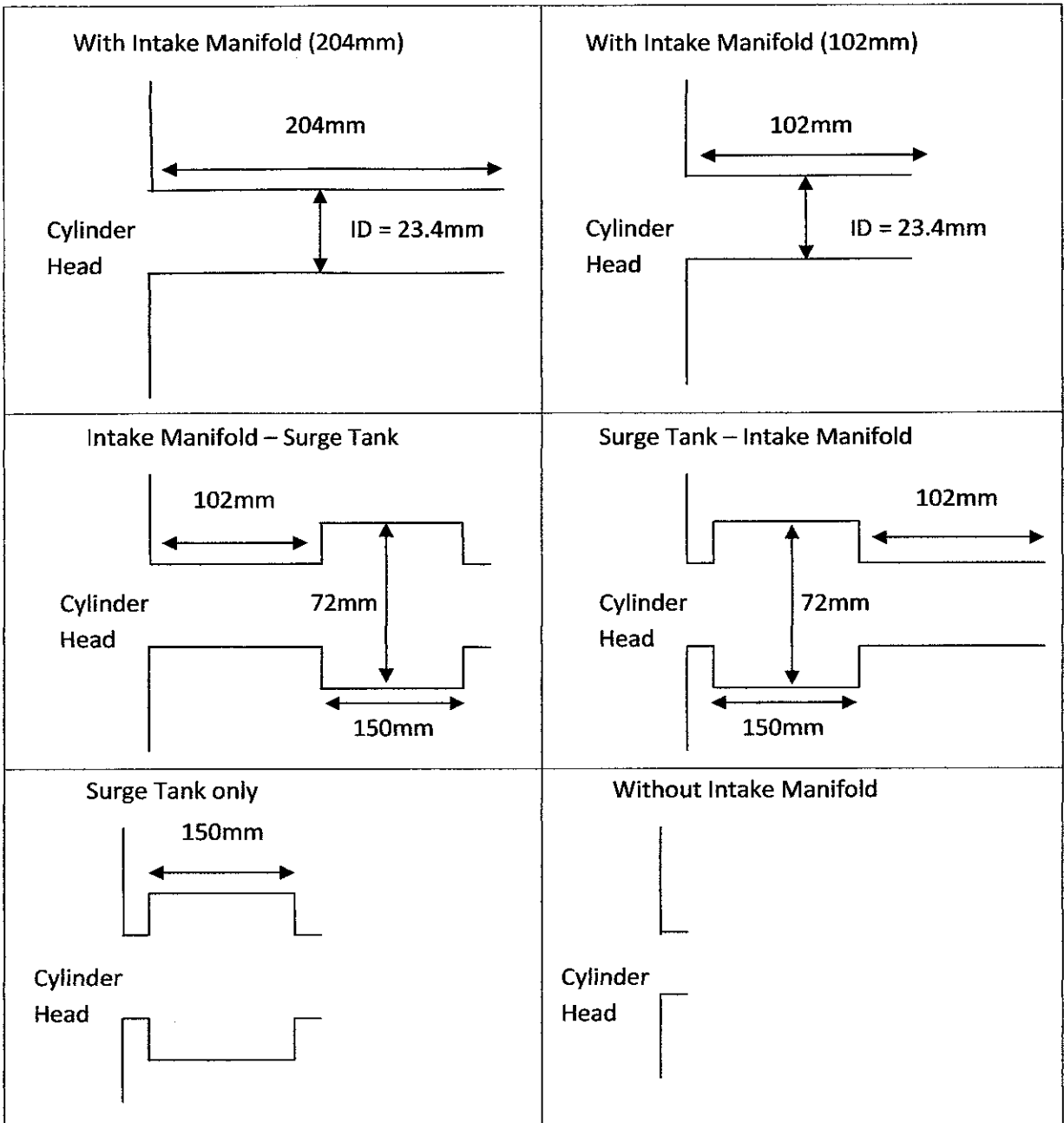


Figure 4.5: Schematic of Variation of Mock Intake Manifold Tested

Figure 4.5 shows the variation of mock intake manifold tested during the experiment. The experiment was conducted with many variations to see the effect of specific geometry towards the air flow pattern. Some geometry gives better mass flow rate of air entering the combustion chamber where as some might cause restriction. This is important as the target is to increase the volumetric efficiency of the engine. The variation of geometry will then be remodeled in CATIA V5 to be analyzed.

## 4.3 Result & Discussion

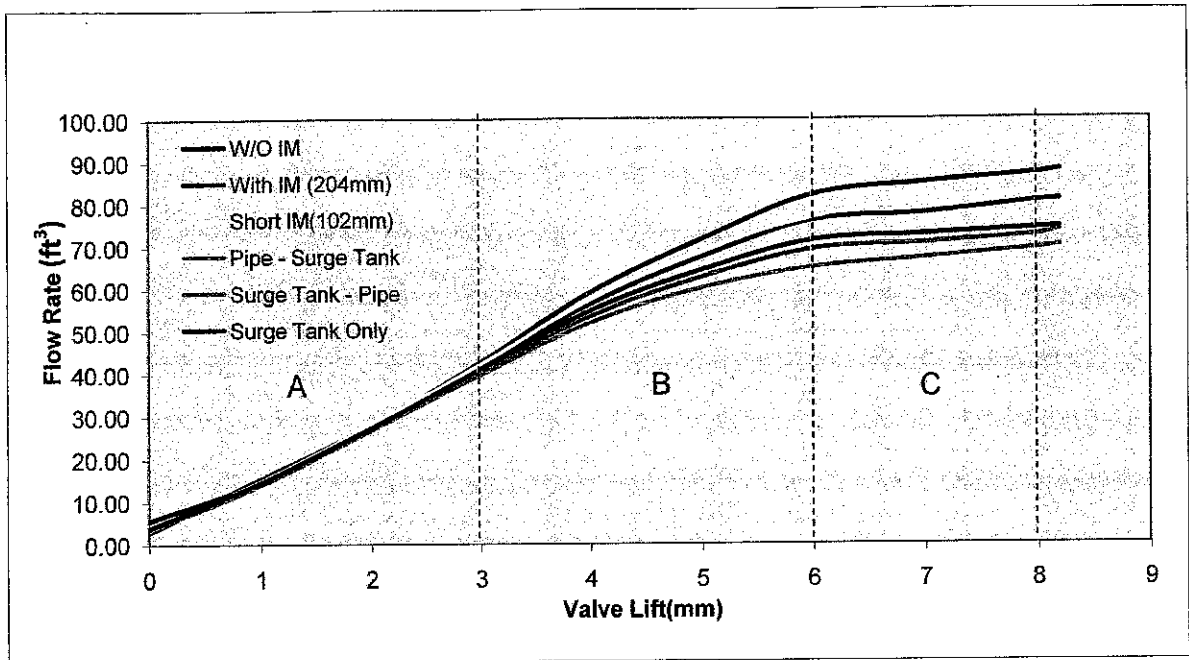


Figure 4.6: Variation of flow rate of air with the valve lift positions for various designs

### 4.3.1 Regime 'A' (0-3mm)

From the graph, it is shown that the trend of increment looks similar for all test variation. The difference of values is quite small. The average of mass flow rate at 3mm valve lift is 41.38 cubic feet. At this condition it is suspected that the air coming into the combustion chamber only have limited area to disperse itself. The variation did not give any significant change as the air enters all at almost the same mass flow rate.

#### **4.3.2 Regime 'B' (3-6mm)**

At this column, the graph shows the start of change of slope for different variation of intake manifold. The mass flow rate increases drastically for the one without intake manifold. This area may be the decisive area at which the design of intake port and intake manifold could determine the maximum mass flow rate into the combustion chamber. It is suspected that at about 5 to 6mm opening of intake valve, the air has the freedom of moving at higher velocity given the same amount of negative pressure at downstream of flow. The reason to this may also be because of the valve profile which causes the drastic increment of surface area when the valve moves downward.

#### **4.3.3 Regime 'C' (6-8.2mm)**

From the graph we can see that the slope for all intake manifold variation remains almost the same up till the last valve opening. The Intake manifold variation did not cause any significant change at this area of column. The mass flow rate increases at almost constant rate because the valve profile did not affect the change in surface area. The end result shows that the one without the intake manifold has the highest flow rate into the combustion chamber.

#### **4.3.4 Discussion**

From the design of the intake port, it shows that without intake manifold seems to give the highest amount of air into the combustion chamber. However it is not possible for an engine to not have an intake manifold. This is because the best combustion happens only when the air-fuel mixture is very thorough. This will cause atomization that enhances the amount of power to the engine and lower the emission rate. Normally an engine places the fuel injector at the upstream to give a better atomization rate of air and fuel but the setback would be in packaging wise.

## CHAPTER 5

### CFD RESULTS AND VALIDATION

#### 5.1 Flow Coefficient Calculation Method

The flow coefficient,  $\alpha_k$  is given by:

$$\alpha_k = \frac{\dot{m}_{real}}{\dot{m}_{theoretical}} \quad (5.1)$$

From the flowbench test, pressure is measured on the rig and the real mass flow rate,  $\dot{m}_{real}$ , in the intake port is calculated by:

$$\dot{m}_{real} = \dot{V} \frac{P}{RT} \quad (5.2)$$

The theoretical mass flow rate  $\dot{m}_{theoretical}$  is calculated using the following equation:

$$\dot{m}_{theoretical} = \rho_s A_k v_s \quad (5.3)$$

$$v_s = \sqrt{\frac{2\gamma}{\gamma-1} RT \left[ 1 - \left[ \frac{P_2}{P_1} \right]^{\frac{\gamma-1}{\gamma}} \right]} \quad (5.4)$$

Where  $\dot{V}$  is volume flow, R is gas constant for air,  $A_k$  equals valve seat area,  $\rho_s$  is the isentropic air density,  $v_s$  is the isentropic flow velocity,  $P_1$  represents air pressure at upstream,  $P_2$  represents air pressure at downstream,  $\gamma$  is the air isentropic exponent.

## 5.2 Example calculations of test without intake manifold at maximum valve lift

Isentropic Flow Velocity is calculated by using the pressure difference from the experiment. From equation 5.4, isentropic velocity,  $v_s$  is calculated by using  $R$  equals 287 Joules;  $T$  equals 293.15 Kelvin,  $P_1$  is the ambient pressure,  $P_2$  is the downstream pressure in the flow bench. The velocity of air entering the intake manifold,  $v_s$ :

$$v_s = 91.767 \text{ m/s}$$

From equation 5.3, theoretical mass flow rate,  $\dot{m}_{theoretical}$  is calculated by multiplying with engine valve seat area,  $A_k$  and experimental air density,  $\rho_s$  with isentropic air velocity,  $v_s$ . Theoretical mass flow rate,  $\dot{m}_{theoretical}$  equals:

$$\dot{m}_{theoretical} = 0.071922 \frac{\text{kg}}{\text{s}}$$

Calculation for flow bench test mass flow rate will be from the gas law which is equation 5.2. Volume flow rate parameter was measured from experiment. Flow rate,  $\dot{V}$ , Pressure Downstream,  $P$  and Temperature,  $T$  are taken from Table 5.1. Experimental mass flow rate,  $\dot{m}_{real}$  equals:

$$\dot{m}_{real} = 0.042902 \frac{\text{kg}}{\text{s}}$$

Flow Coefficient,  $\alpha_k$  can be calculated using equation 5.1 by utilizing the previous calculated theoretical mass flow rate,  $\dot{m}_{theoretical}$  and experimental mass flow rate,  $\dot{m}_{real}$ . Flow Coefficient,  $\alpha_k$  equals:

$$\alpha_k = 0.59650$$

From the experiment and analysis, data was collected and tabulated in Tables 5.1 to 5.6. The table represents each of the geometry variations of the intake manifold. Only test pressure, experimental flow rate and test temperature data were measured and collected from the experiment. FLUENT analysis validation was done for two variations which were the engine without intake manifold and with a 204 mm intake manifold.

The geometry difference for all experiments gave different readings of mass flow rate. From the comparison of Tables 5.3 and 5.4, the flow rate is slightly higher for the intake manifold without the surge tank. However, the surge tank could reduce the turbulence intensity as the air enters the intake manifold.

Table 5.1: Experiment 1 Engine without Intake Manifold

Valve Lift(mm)	Test Pressure (inH <sub>2</sub> O)	Test Temperature in Celsius	Calculated Air Density (kg/m <sup>3</sup> )	Experiment al Flow Rate (Cubic Feet per minute)	Experiment Flow Rate (Cubic meter per second)	Experiment Mass Flow Rate(Kg/s)	Mass Flow Rate CFD FLUENT (Kg/s)	Calculated Theoretical Mass Flow Rate(Kg/s)	Flow Coefficient Experiment	Flow Coefficient CFD FLUENT	L/D	Percentage Diference (%)	Calculated Isentropic Velocity(m/s)
First Try Without intake manifold													
0	19.98	29.222	1.1077	2.70	0.0013	0.0014	0.0014	0.0663	0.021	0.022	0.000	1.035	93.1998
1	19.97	33.278	1.0930	15.40	0.0073	0.0079	0.0095	0.0659	0.121	0.145	0.035	16.777	93.8227
2	19.97	35.222	1.0861	27.90	0.0132	0.0143	0.0179	0.0657	0.218	0.272	0.070	19.907	94.1200
3	19.96	37.056	1.0797	42.70	0.0202	0.0218	0.0272	0.0655	0.332	0.415	0.105	20.020	94.3993
4	19.96	39.722	1.0705	59.00	0.0278	0.0298	0.0350	0.0652	0.457	0.537	0.140	14.798	94.8042
5	19.96	42.333	1.0617	71.50	0.0337	0.0358	0.0408	0.0649	0.552	0.628	0.175	12.089	95.1990
6	19.95	44.056	1.0559	82.10	0.0387	0.0409	0.0456	0.0648	0.632	0.704	0.210	10.298	95.4585
7	19.96	46.722	1.0471	85.00	0.0401	0.0420	0.0505	0.0645	0.651	0.783	0.245	16.787	95.8589
8	19.96	49.556	1.0379	87.10	0.0411	0.0427	0.0532	0.0642	0.665	0.828	0.280	19.751	96.2825
8.2	19.96	51.444	1.0319	87.90	0.0415	0.0428	0.0540	0.0640	0.669	0.843	0.287	20.715	96.5639

Table 5.2: Experiment 2 Engine Assembly with 204mm Intake Pipe

Valve Lift(mm)	Test Pressure (inH <sub>2</sub> O)	Test Temperature in Celsius	Calculated Air Density (kg/m <sup>3</sup> )	Experiment al Flow Rate (Cubic Feet per minute)	Experiment Flow Rate (Cubic meter per second)	Experiment Mass Flow Rate(Kg/s)	Mass Flow Rate CFD FLUENT (Kg/s)	Calculated Theoretical Mass Flow Rate(Kg/s)	Flow Coefficient Experiment	Flow Coefficient CFD FLUENT	L/D	Percentage Diference (%)	Calculated Isentropic Velocity(m/s)
With Intake Manifold (204mm)													
0	19.87	57.278	1.0136	2.70	0.0013	0.0013	0.0013	0.0634	0.020	0.020	0.000	0.642	97.4277
1	19.96	58.389	1.0103	14.70	0.0069	0.0070	0.0077	0.0633	0.111	0.122	0.035	9.307	97.5913
2	19.98	59.056	1.0082	27.90	0.0132	0.0133	0.0155	0.0633	0.210	0.244	0.070	14.107	97.6894
3	19.96	60.444	1.0040	41.80	0.0197	0.0198	0.0245	0.0631	0.314	0.388	0.105	19.255	97.8934
4	19.96	61.722	1.0002	56.30	0.0266	0.0266	0.0317	0.0630	0.422	0.503	0.140	16.112	98.0807
5	19.96	62.722	0.9972	67.40	0.0318	0.0317	0.0373	0.0629	0.504	0.592	0.175	14.912	98.2271
6	19.96	63.778	0.9941	76.10	0.0359	0.0357	0.0419	0.0628	0.568	0.667	0.210	14.831	98.3813
7	19.97	64.667	0.9915	77.90	0.0368	0.0365	0.0464	0.0627	0.581	0.739	0.245	21.441	98.5110
8	19.96	65.444	0.9892	80.60	0.0380	0.0376	0.0476	0.0627	0.600	0.759	0.280	20.949	98.6243
8.2	19.95	66.167	0.9871	80.90	0.0382	0.0377	0.0478	0.0626	0.602	0.764	0.287	21.188	98.7294

Table 5.3: Experiment 3 Engine Assembly with 102mm Intake Pipe

Valve Lift(mm)	Test Pressure(inH2O)	Test Temperature In.Celcius	Calculated Air Density(kg/m3)	Experimental Flow Rate (Cubic Feet per minute)	Experiment Flow Rate (Cubic meter per second)	Experiment Mass Flow Rate(Kg/s)	Calculated Theoretical Mass Flow Rate(Kg/s)	Flow Coefficient Experiment	L/D	Calculated Isentropic Velocity(m/s)
Short Pipe										
0	19.97	51.500	1.0317	3.60	0.0017	0.0018	0.0567	0.031	0.000	85.5535
1	19.96	54.778	1.0214	14.90	0.0070	0.0072	0.0564	0.127	0.035	85.9843
2	19.96	56.333	1.0166	28.10	0.0133	0.0135	0.0563	0.240	0.070	86.1880
3	19.97	58.889	1.0087	42.30	0.0200	0.0201	0.0561	0.359	0.105	86.5216
4	19.98	61.556	1.0007	57.30	0.0270	0.0271	0.0558	0.485	0.140	86.8683
5	19.97	63.444	0.9951	69.00	0.0326	0.0324	0.0557	0.582	0.175	87.1131
6	19.98	65.389	0.9894	76.80	0.0362	0.0359	0.0555	0.646	0.210	87.3644
7	19.93	67.000	0.9847	81.00	0.0382	0.0376	0.0554	0.680	0.245	87.5720
8	19.96	68.500	0.9804	83.20	0.0393	0.0385	0.0553	0.696	0.280	87.7649
8.2	19.97	69.500	0.9775	83.80	0.0395	0.0387	0.0552	0.700	0.287	87.8932

Table 5.4: Experiment 4 Engine Assembly with 102mm Intake pipe and a Surge Tank

Valve Lift(mm)	Test Pressure(inH2O)	Test Temperature In.Celcius	Calculated Air Density(kg/m3)	Experimental Flow Rate (Cubic Feet per minute)	Experiment Flow Rate (Cubic meter per second)	Experiment Mass Flow Rate(Kg/s)	Calculated Theoretical Mass Flow Rate(Kg/s)	Flow Coefficient Experiment	L/D	Calculated Isentropic Velocity(m/s)
Pipe with Surge Tank										
0	19.96	49.889	1.0368	3.30	0.0016	0.0016	0.0568	0.028	0.000	85.3409
1	19.97	52.889	1.0273	14.00	0.0066	0.0068	0.0566	0.120	0.035	85.7363
2	19.97	54.889	1.0210	26.90	0.0127	0.0130	0.0564	0.230	0.070	85.9989
3	19.97	57.500	1.0130	39.80	0.0188	0.0190	0.0562	0.339	0.105	86.3405
4	19.96	60.500	1.0039	51.90	0.0245	0.0246	0.0559	0.440	0.140	86.7313
5	19.95	62.722	0.9972	60.10	0.0284	0.0283	0.0557	0.507	0.175	87.0196
6	19.94	64.333	0.9925	65.00	0.0307	0.0304	0.0556	0.547	0.210	87.2281
7	19.96	65.722	0.9884	67.30	0.0318	0.0314	0.0555	0.566	0.245	87.4074
8	19.96	67.000	0.9847	69.50	0.0328	0.0323	0.0554	0.583	0.280	87.5720
8.2	19.95	67.944	0.9819	70.10	0.0331	0.0325	0.0553	0.587	0.287	87.6935

Table 5.5: Experiment 5 Engine Assembly with 102mm Intake Pipe and a Surge Tank (Pipe at Upstream)

Valve Lift(mm)	Test Pressure(inH2O)	Test Temperature in Celsius	Calculated Air Density(kg/m <sup>3</sup> )	Experimental Flow Rate (Cubic Feet per minute)	Experiment Flow Rate (Cubic meter per second)	Experiment Mass Flow Rate(Kg/s)	Calculated Theoretical Mass Flow Rate(Kg/s)	Flow Coefficient Experiment	L/D	Calculated Isentropic Velocity(m/s)
Surge Tank with Pipe										
0	19.96	60.778	1.0030	3.40	0.0016	0.0016	0.0559	0.029	0.000	86.7673
1	19.95	62.611	0.9975	14.60	0.0069	0.0069	0.0558	0.123	0.035	87.0052
2	19.97	63.833	0.9939	27.40	0.0129	0.0129	0.0557	0.231	0.070	87.1634
3	19.96	66.444	0.9863	40.60	0.0192	0.0189	0.0554	0.341	0.105	87.5005
4	19.97	66.389	0.9807	53.40	0.0252	0.0247	0.0553	0.447	0.140	87.7506
5	19.96	69.944	0.9762	62.60	0.0295	0.0288	0.0552	0.523	0.175	87.9502
6	19.95	71.111	0.9729	69.30	0.0327	0.0318	0.0551	0.578	0.210	88.0996
7	19.96	72.222	0.9698	70.80	0.0334	0.0324	0.0550	0.589	0.245	88.2417
8	19.97	73.222	0.9670	72.60	0.0343	0.0331	0.0549	0.604	0.280	88.3693
8.2	19.95	74.222	0.9642	73.80	0.0348	0.0336	0.0548	0.613	0.287	88.4968

Table 5.6: Experiment 6 Engine Assembly with only a Surge Tank

Valve Lift(mm)	Test Pressure(inH2O)	Test Temperature in Celsius	Calculated Air Density(kg/m <sup>3</sup> )	Experimental Flow Rate (Cubic Feet per minute)	Experiment Flow Rate (Cubic meter per second)	Experiment Mass Flow Rate(Kg/s)	Calculated Theoretical Mass Flow Rate(Kg/s)	Flow Coefficient Experiment	L/D	Calculated Isentropic Velocity(m/s)
Surge Tank only										
0	19.97	64.222	0.9928	3.70	0.0017	0.0017	0.0556	0.031	0.000	87.2137
1	19.98	66.778	0.9853	14.60	0.0069	0.0068	0.0554	0.123	0.035	87.5434
2	19.97	68.722	0.9797	27.40	0.0129	0.0127	0.0553	0.229	0.070	87.7934
3	19.98	71.722	0.9712	41.10	0.0194	0.0188	0.0550	0.342	0.105	88.1778
4	19.95	73.944	0.9650	54.70	0.0258	0.0249	0.0548	0.454	0.140	88.4614
5	19.94	75.444	0.9608	64.30	0.0303	0.0292	0.0547	0.533	0.175	88.6524
6	19.95	76.667	0.9575	71.40	0.0337	0.0323	0.0546	0.591	0.210	88.8076
7	19.94	77.500	0.9552	72.90	0.0344	0.0329	0.0546	0.602	0.245	88.9134
8	19.96	78.389	0.9528	74.20	0.0350	0.0334	0.0545	0.612	0.280	89.0260
8.2	19.95	78.889	0.9514	74.50	0.0352	0.0335	0.0545	0.614	0.287	89.0893

## 5.3 Test Data Validation

### 5.3.1 Without Intake Manifold

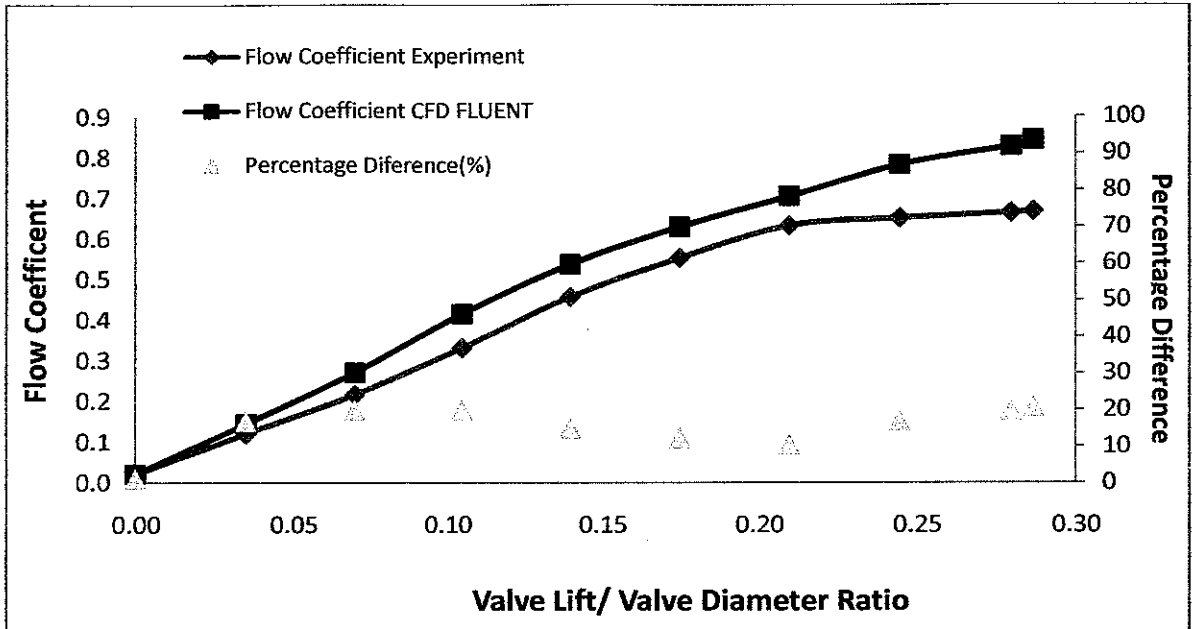


Figure 5.1: Graph of Flow Coefficient Comparison of Engine without Intake Manifold between CFD and Experimental Data

Figure 5.1 shows the comparison of flow coefficient into combustion chamber between experimental and computed CFD in FLUENT. The engine setup for this experiment is with maximum valve lift of 8.2 mm and wide open throttle. The real test shows a higher flow coefficient throughout the whole valve opening. This may be because of the difference in geometry of the intake port and the intake valve. The correlation shows that the flow coefficient from CFD is higher than the experimented at similar valve lift/diameter ratio. The flow coefficient values at 8.2 mm differ by 0.174. The CFD model has under predicted the flow coefficient by 20.64%.

$$\text{Percentage Difference} = \frac{C_{f,m} - C_{f,p}}{C_{f,m}} \times 100\% \quad (5.5)$$

where  $C_{f,m}$  is measured flow coefficient and  $C_{f,p}$  is predicted flow coefficient. Percentage difference equals:

$$\text{Percentage Difference} = 20.64\%$$

### 5.3.2 With Intake Manifold (204mm)

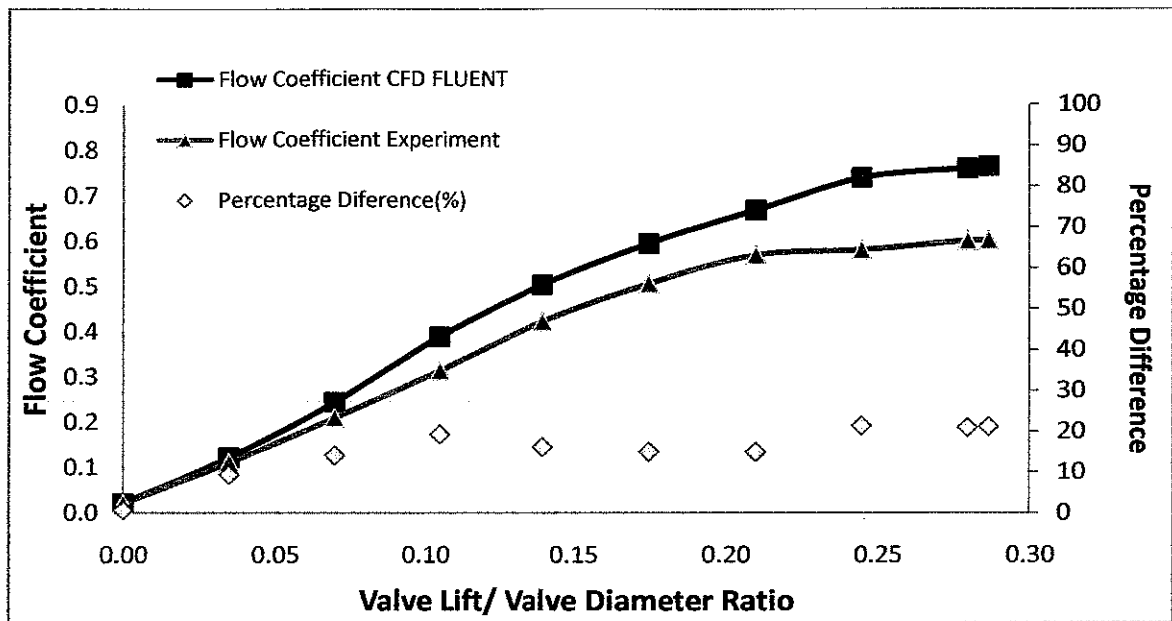


Figure 5.2: Graph of Flow Coefficient Comparison of Engine with 204mm Intake Pipe between CFD and Experimental Data

Figure 5.2 shows the comparison of flow coefficient into combustion chamber with the constraint of 204 mm intake manifold between experimental and computed CFD in FLUENT. The engine setup for this experiment is with maximum valve lift of 8.2 mm and wide open throttle. Again the values of CFD flow coefficient are higher than the experimental throughout the entire valve lift.

The correlation shows that the actual measured flow coefficient is lower than the predicted at similar valve lift/diameter ratio. The flow coefficient values at 8.2 mm differ by 0.162. The CFD model has under predicted the flow coefficient by 21.2%.

$$\text{Percentage Difference} = \frac{C_{f,m} - C_{f,p}}{C_{f,m}} \times 100\% \quad (5.6)$$

where  $C_{f,m}$  is measured flow coefficient and  $C_{f,p}$  is predicted flow coefficient. Percentage difference equals:

$$\text{Percentage Difference} = 21.2\%$$

## 5.4 Discussion of Validation

The following key findings can be highlighted from the port flow CFD simulation and its validation process, which may be accountable for the unusual difference. It is important to create an accurate experimental setup in the CFD model and match all the correct boundary conditions. In this analysis, the geometrical difference may be the factor to the higher or lower flow coefficient comparison. The 3D model may not be the same as some defects must have occurred during the fabrication period. The cylinder head was sand casted and this characteristic is not accounted in the CFD analysis.

During the experiment, the test product used was not fabricated but instead was bought as standard part. Therefore there was no proper mounting used connected to the engine. The test piece was mounted to the engine using clay covering the area around the pipe opening. This may cause disturbance to the flow rate as the clay may have changed the cross sectional area of the pipe. Other than that, there may be uncertainty in the flow bench rig. There was no calibration conducted prior to the test done. This could lead to difference in pressure boundary condition that has been set during the experiment. If the pressure setting is not accurate as wanted, the velocity of flow coming in may differ, hence offsetting the volume flow rate as well. Since the measured flow rate is considered quite small, the slightest of change may cause big difference compared to the CFD model. Renolds Number in Pipe:

$$Re = \frac{\rho V_{avg} D}{\mu} \quad (5.7)$$

$$Re = \frac{\left(1.22 \frac{kg}{m^3}\right) \left(91.767 \frac{m}{s}\right) (0.0286m)}{1.825e^{-5} \frac{kg}{ms}}, \text{ Velocity value from example calculation}$$

$$Re = 175448$$

The flow in pipe is a turbulent as the renolds number exceeds 4000. The simulation will only be conducted in turbulent characteristics.

### 5.5 Calculation of Entrance Region to the pipe

The fluid particles in the layer in contact with the surface of the pipe come to a complete stop. This layer also causes the fluid particles in the adjacent layers to slow down gradually as a result of friction. To make up for this velocity reduction, the velocity of the fluid at the mid section of the pipe has to increase to keep the mass flow rate through the pipe constant. The region of flow in which the effects of the viscous shearing forces caused by the fluid viscosity are felt is the velocity boundary layer. In the boundary layer the viscous effects and velocity changes are significant. For the fluid flow in the entrance region of a pipe, the wall shear stress is the highest at the pipe inlet where the thickness of the boundary layer is smallest. Therefore the pressure drop is higher at the entrance region of a pipe.

The hydrodynamic entry length which is the region from the pipe inlet to the point at which the boundary layer merges at the centerline for the turbulent flow can be approximated as:

$$L_{h,turbulent} = 1.359DRe_D^{1/4} \quad (5.8)$$

$$L_{h,turbulent} = 1.359 (0.0286m)(35566)_D^{1/4}$$

$$L_{h,turbulent} = 0.5337m$$

The calculated entry length is calculated to be about 0.533 m and this cannot be achieved because the intake pipe has only a maximum length of 0.3 m. The velocity profile will not be able to develop fully as there is not enough length of pipe. Figure 5.4 shows the velocity profile of air coming into the combustion chamber.

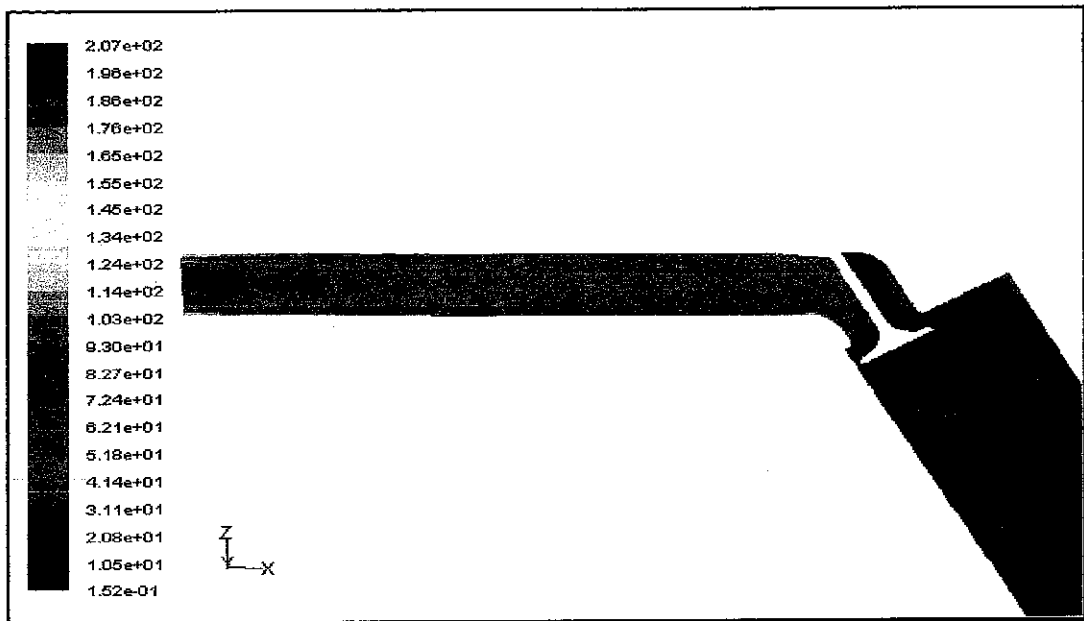


Figure 5.3: Boundary Layer shown in FLUENT

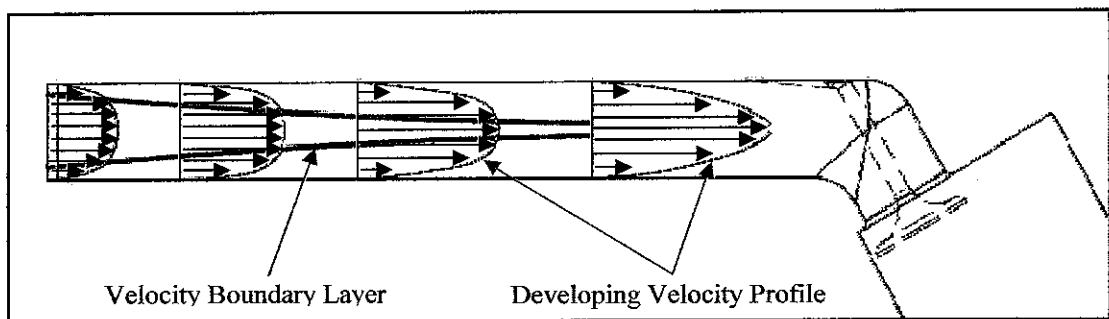


Figure 5.4: Illustration of Boundary Layer

Figure 5.3 shows the boundary layer of air developed in the intake manifold. The illustration in Figure 5.4 shows that the boundary layer has not developed completely. This is because there is not enough length for the velocity profile to be fully developed. The boundary layer may be differently developed for different air intake manifold geometry. The surface roughness of the intake manifold also determines the pattern of the boundary layer.

## CHAPTER 6

### PROTOTYPE DESIGN

The idea of designing air intake manifold is to house the electronic fuel injector while maintaining the current engine performance or even to improve it if possible. Other than that, it is important to make sure that the design complies with the packaging requirement of the Go-Kart assembly.

The study aims to differentiate the characteristics of air entering the combustion chamber with different design of intake manifold. The characteristics are such as mass flow rate of air entering, swirl coefficient and air-fuel mixture content. With the changes in air intake manifold characteristics, there are potentials that the mass flow rate coming into the combustion chamber may be increased. The proposed designs study is shown in Figure 6.1.

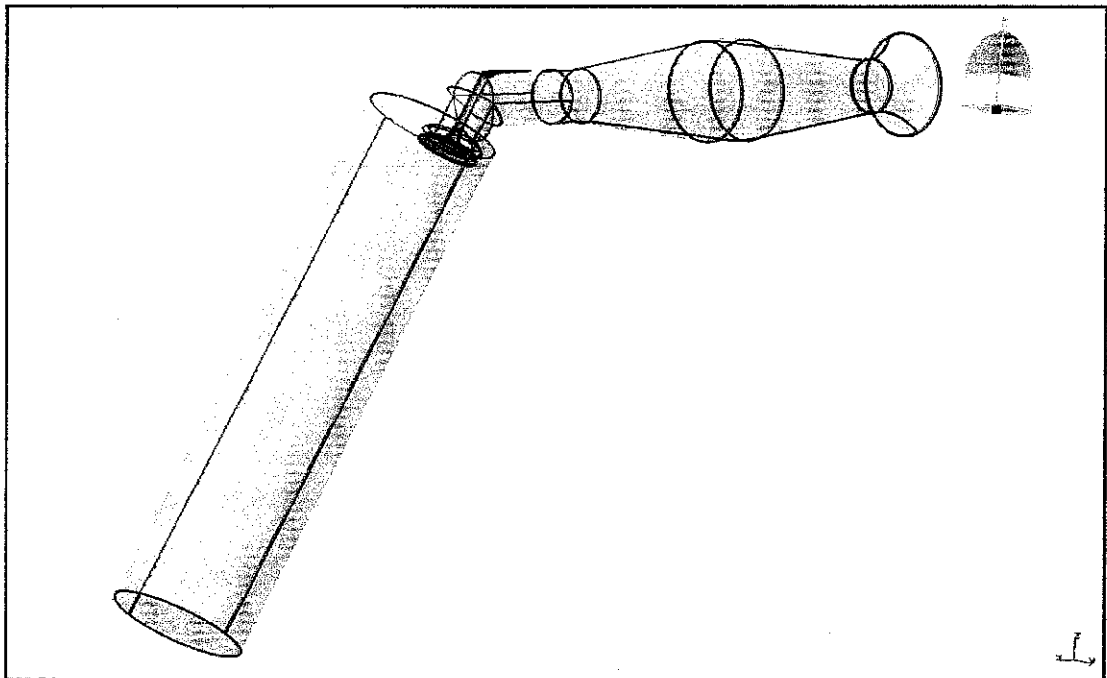


Figure 6.1: Isometric View of Air Intake Path of the New Proposed Design

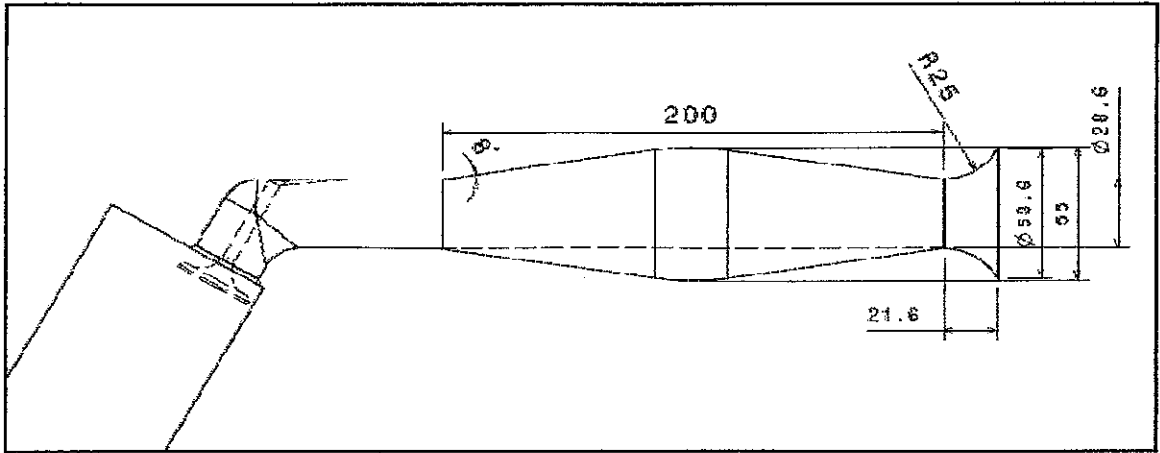


Figure 6.2: Dimension of the side cross sectional area of the intake manifold

### 6.1 Diffuser to Nozzle Shape

The presence of tapered pipes in engine intake manifold is to act as a nozzle or diffuser. This will help produce gradual process of reflection of pressure waves experienced rather than abrupt change in cross sectional area. This process is more efficient at reflecting wave energy because it is spread out in terms of time. Any ensuing tuning effect on the engine is not only more pronounced but is effective over wider speed range. The reason of having a diffuser in the beginning is to facilitate the air movement so that it could reduce the turbulent intensity. Figure shows the dimension of the side cross sectional area of the diffuser and nozzle pattern. The air going to through the diffuser would then be channeled to a nozzle to increase the velocity of air coming into the combustion chamber. This would aid the atomization of the fuel and air mixture before being combusted.

### 6.2 Bellmouth Shape

The use of bellmouth at the end of an intake pipe is the conventional method employed to improve the mass flow rate of flow of air into the intake pipe from the atmosphere. The design of the bellmouth gives better opportunity for air to be trapped in the pipe hence increasing the mass flow rate of suction. This design is targeted to increase the mass flowrate of the intake pipe by at least 5% or more. If the bellmouth is used for this application, the engine need to have a different filter to make sure that debris do not go into the combustion chamber.

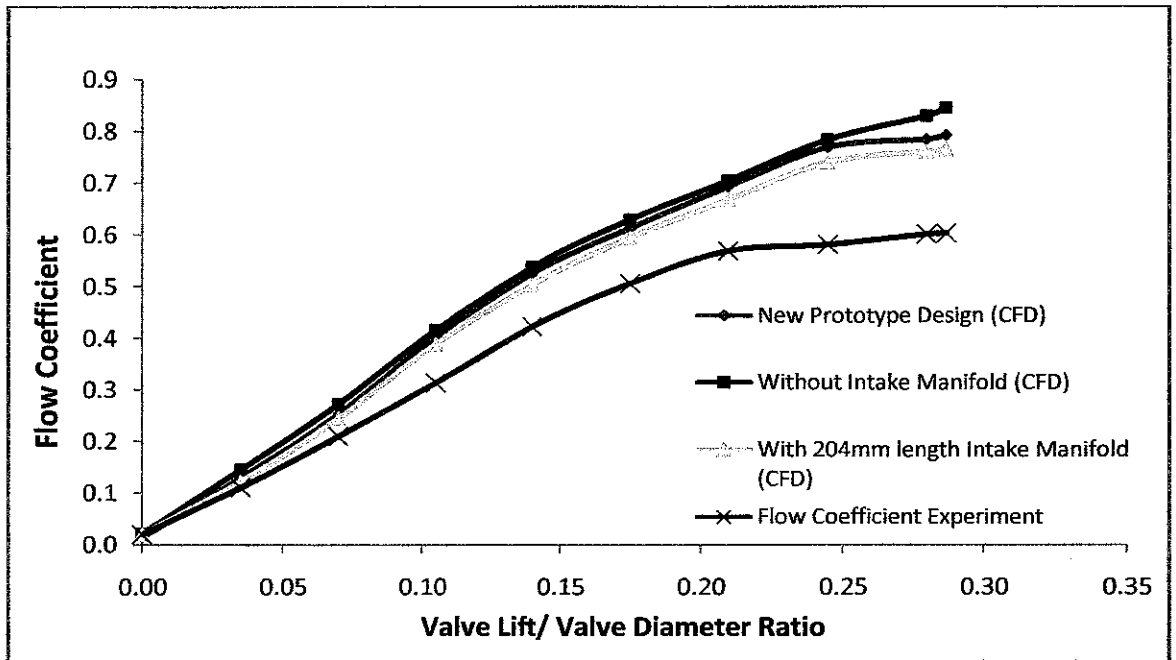


Figure 6.3: Graph comparison of flow coefficient vs valve lift/diameter

### 6.3 Comparison of Flow Coefficient of New Prototype Design

Figure 6.3 shows the comparison of flow coefficient between CFD and real Experiment. From the graph above, we can see that the CFD flow coefficient is much higher than the experimental results. It seems that the CFD results from FLUENT over predicted the results. This situation has been discussed in the previous results. For this graph, it is the comparison between the various CFD models that is important. From the results, it shows that the new prototype design gives higher flow coefficient compared to other design of intake manifold; i.e. 204 mm intake manifold. The amount of air coming into the combustion chamber at one time is more by using the new prototype intake manifold design. At valve lift of 2 mm the prototype shows a vast improvement in the amount mass flow rate of air. For an engine, normally the air intake performs better when there is no intake manifold because there is no restriction. However the new intake design can provide even higher flow coefficient than that without the intake manifold.

## CHAPTER 7

### CONCLUSIONS AND RECOMMENDATIONS

The project was basically about optimizing the air intake manifold of a newly designed electronic fuel injection conversion of the engine. Appropriate steps were taken to ensure that the research and simulation could be done orderly. This was important since if the results shows an increase in volumetric efficiency and swirl and tumble coefficient, the torque or power output could be increased as well. By varying the intake manifold pipe geometry, it is possible to have an optimum length at which the engine could perform well at a wide range of RPM. A flow bench was used to validate the prediction from the CFD analysis. From the data it was shown that the CFD results were always over predicted. Even though the results of CFD and real test differ a lot, the pattern of the graph remains almost the same. In the project, a new intake manifold was designed utilizing a bell mouth and diffuser shape. From the CFD analysis of the new intake manifold design it was shown that there were increases in the flow coefficient. The new design of the intake manifold may be suitable for use with the K200 engine as it is better than the normal straight pipe design. The CFD results were validated with the experimental results obtained by utilizing the flow bench. Although well validated, it is recommended that the experiment should be done again in the future with appropriate procedure and tools to get more accurate comparison. At the same time the designs were carefully looked into for installation of the electronic fuel injector. At the end of the research, the air intake manifold holds two main purposes which are to facilitate as much air travels into the combustion chamber and also to hold the electronic fuel injector. With a successful conversion, it is likely that the engine will have a better performance

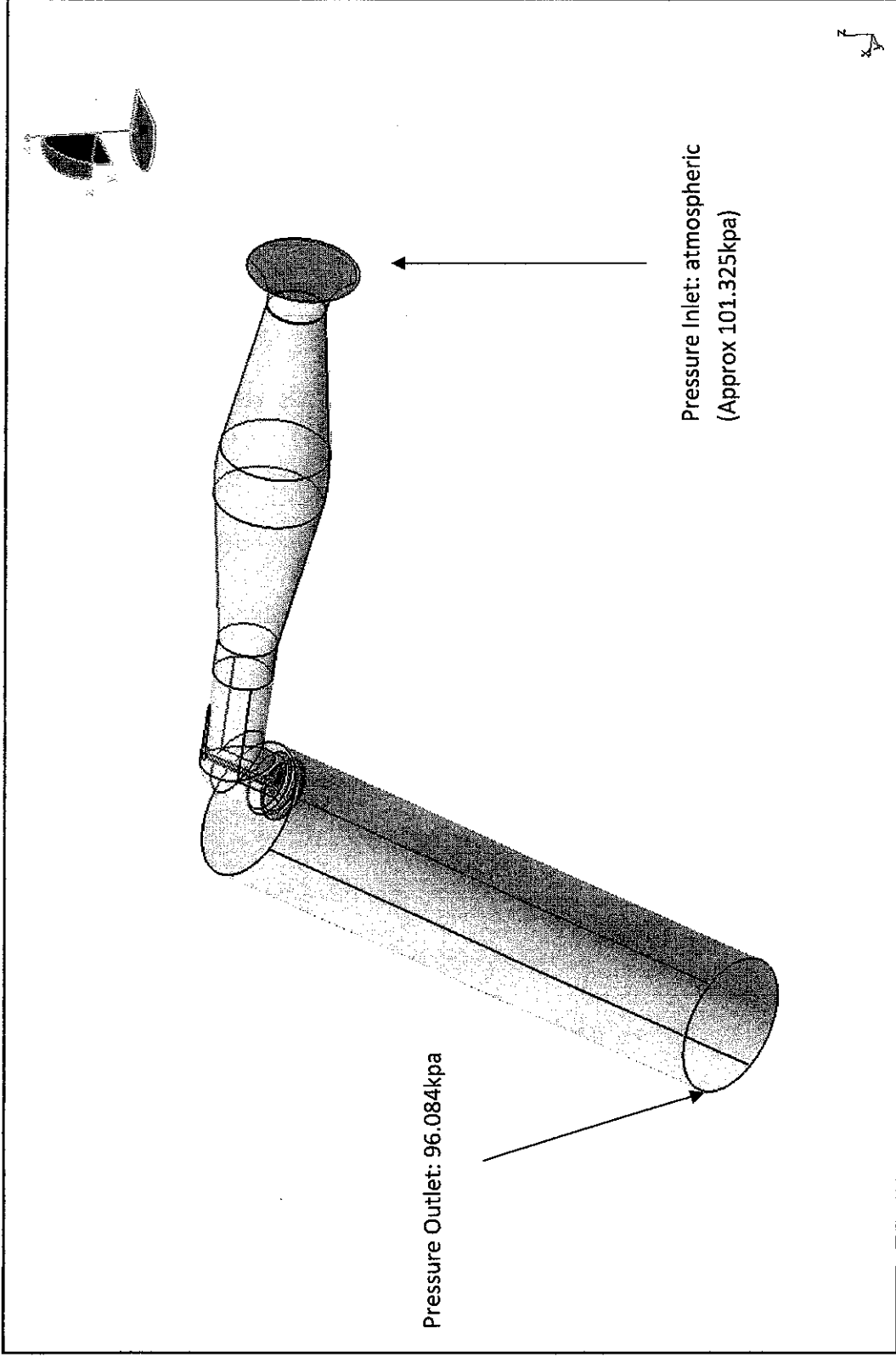
The flow bench test gives the indication that there are areas where energy losses could be found. The CFD analysis has over predicted for most of the test. For future works, it is recommended that the CFD simulation is given a more detail parameters to make

the analysis even more accurate. The parameters that might be considered in the future are temperature of air and detailed surface roughness of the whole system. Other than that, the geometry of the engine should be looked into again to make sure that they are similar. Another thing is that the flow bench test should be done in a more thorough manner. Prior to the experiment the flow bench machine should be calibrated and a proper mock intake manifold should be fabricated. This could improve the accuracy of the data validation. Once the targeted pipe geometry variation is achieved, the next step is to simulate the mixture of fuel injection with the air into the combustion chamber. This however would need a little study on the capability of the FLUENT software. The other concern is the parameters of the electronic fuel injection. The simulation should show the mixture motion of fuel and air with various amount of pressure applied by the injector. The electronic fuel injector should be carefully selected based on the requirement of the engine. The intake manifold could be designed in a more detailed manner once the simulation is complete to ensure that the mounting position of the electronic fuel injector is well placed.

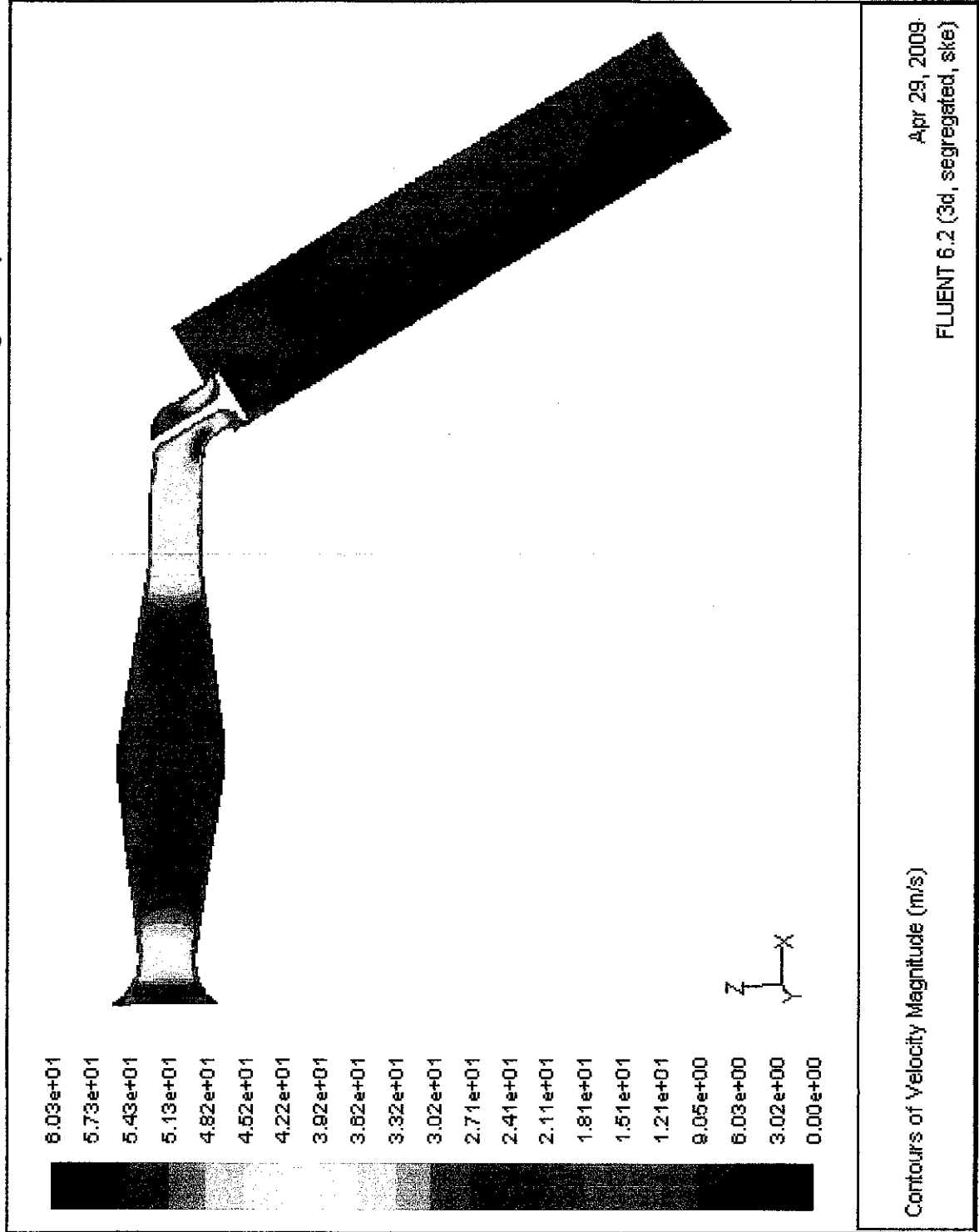
## REFERENCES

- Amer, A. A., & Reddy, T. N. (2002). Multidimensional Optimization of In-Cylinder Tumble Motion for the New Chrysler Hemi. *Society of Automotive Engineers, Inc* , 87-95.
- Crouse, W. H., & Anglin, D. L. (1993). *Automotive Mechanics Tenth Edition*. McGraw-Hill International Editions.
- Fontana, G., Galloni, E., Jannelli, E., & Palmaccio, R. (2003). Influence of the Intake System Design on a Small Spark-Ignition Engine Performance A Theoretical Analysis. *Society of Automotive Engineers, SAE Inc* , 123-130.
- Ghazali, K. I., & Ahmad, A. (2004). *Flowbench Testing*. Sauber PETRONAS Engineering.
- Halderman, J. D., & Jr, C. D. (2005). *Automotive Engines, Theory and servicing*. Prentice Hall.
- James, O. D. (2004). <http://www.gokartracer.com>. Retrieved August 2008, from Gokartracer.
- Laramee, R. S., Weiskopf, D., Schneider, J., & Hauser, H. (2004). Investigating Swirl and Tumble Flow with a Comparison of Visualization Techniques. 1-8.
- McLandress, A., Emerson, R., McDowell, P., & Rutland, C. J. (2005). Intake and In-Cylinder Flow Modeling. *Characterization of Mixing and Comparison with Flow Bench Results*, 1-13.
- Nor, M. F. (2004). *Port Flow CFD Simulation*. Sauber PETRONAS Engineering.
- Pulkrabek, W. W. (2004). *Engineering Fundamentals of the Internal Combustion Engine*. Pearson, Prentice Hall.
- Rathnaraj, J. D., & Kumar, N. (2007). Studies on Variable Swirl Intake System for DI Diesel Engine Using CFD. *International Journal of Applied Engineering Research* , 1-10.
- Srinivasan, S. (2001). *Automotive Engines*. New Delhi: Tata McGraw Hill.
- Winterbone, D. E., & Pearson, R. J. (1999). *Design Techniques for Engine Manifolds, Wave action Methods for IC Engines*. Society of Automotive Engineers (SAE), Inc.

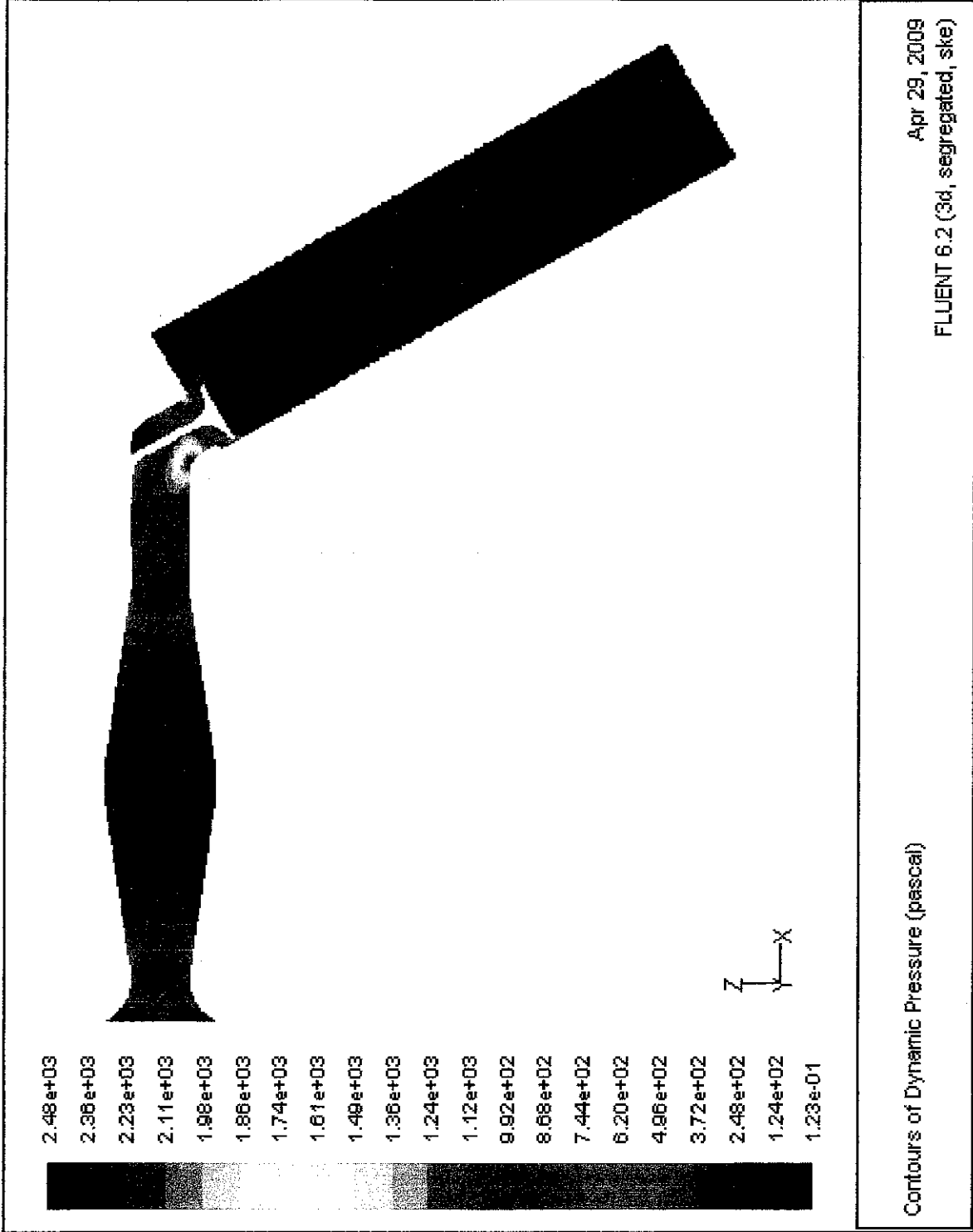
Appendix A: Applied Boundary Conditions for CFD simulation



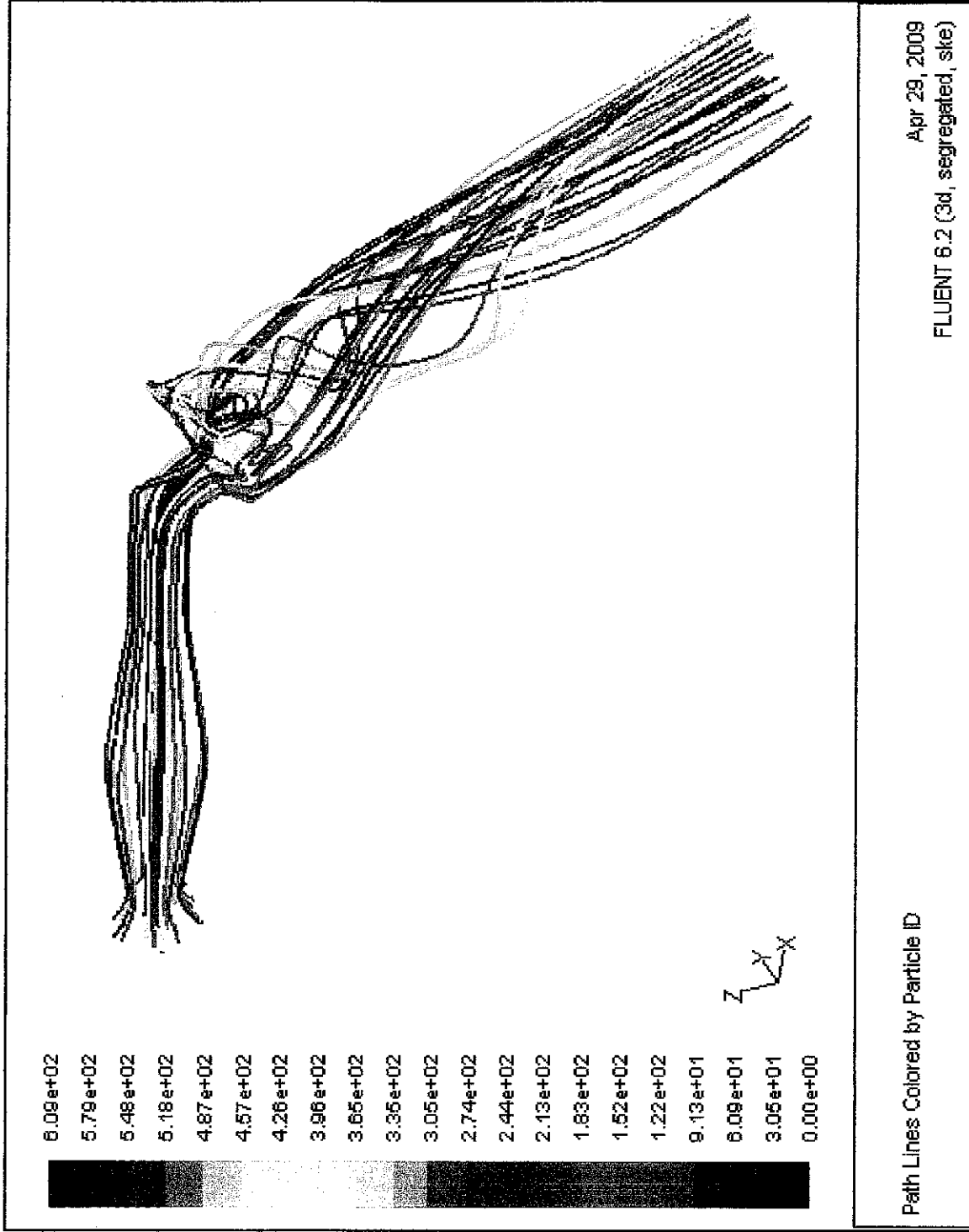
Appendix B: CFD Velocity Plot of New Intake Manifold Design Analysis



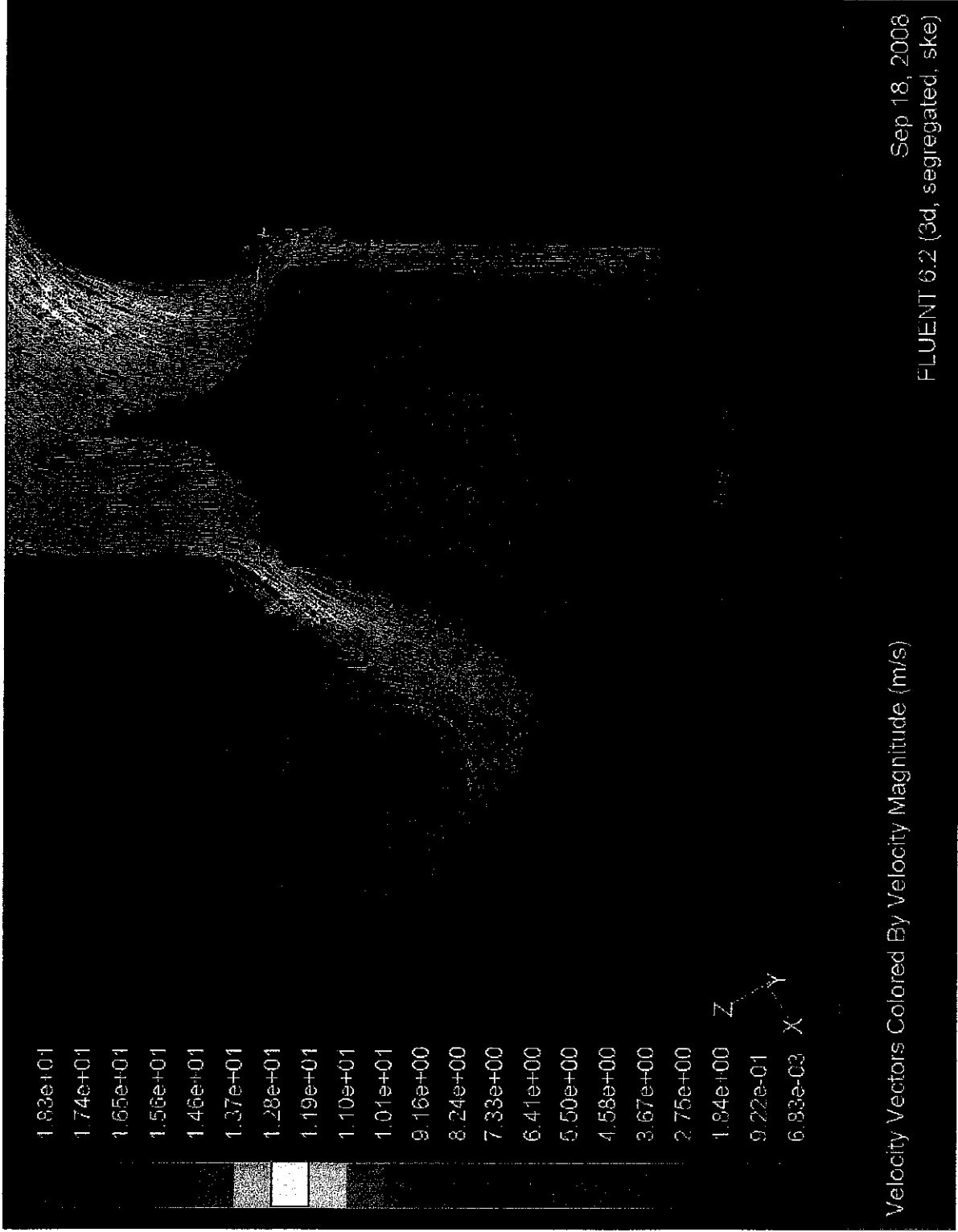
Appendix C: CFD Pressure Plot of New Intake Manifold Design Analysis



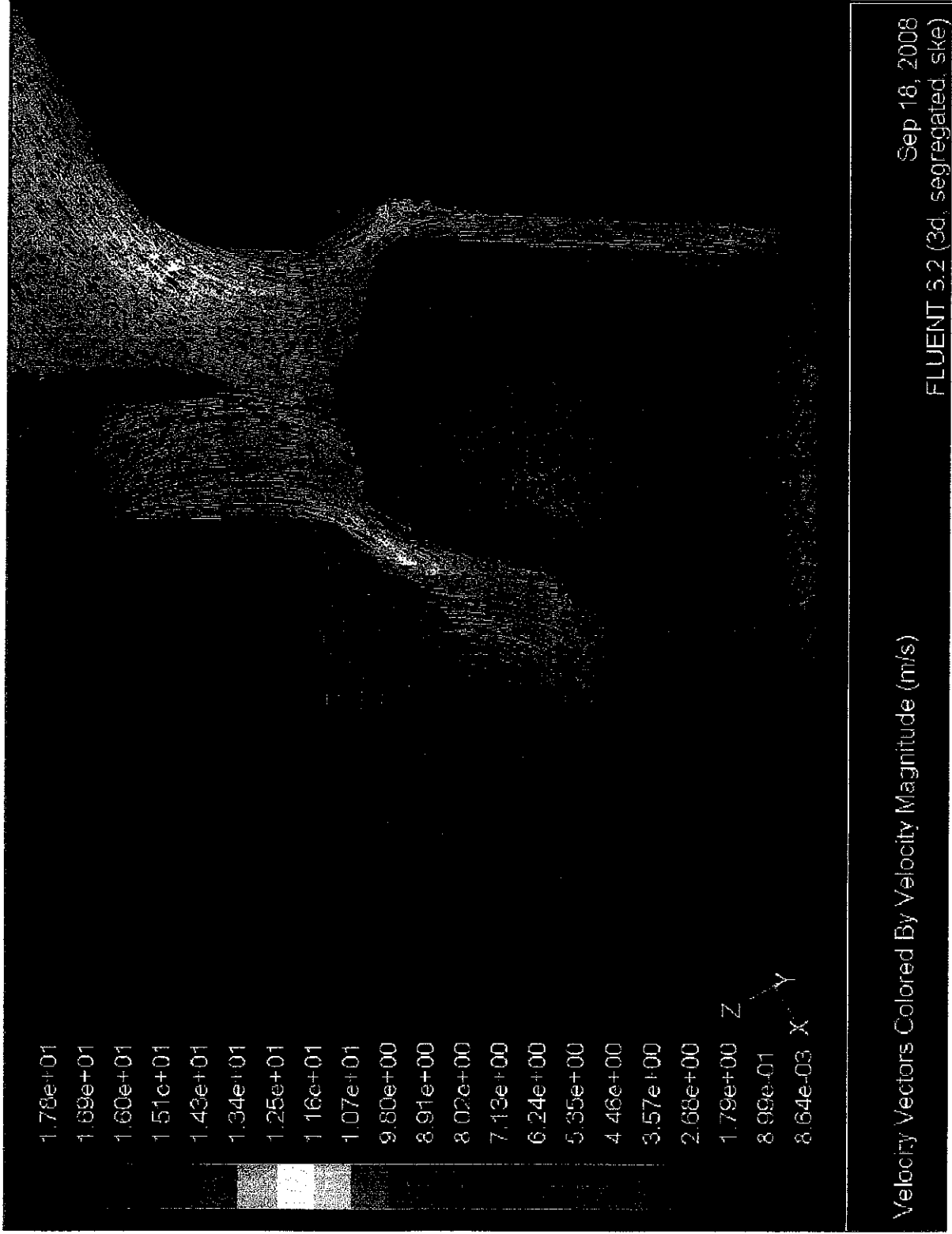
Appendix D: Particle Tracking from CFD simulation



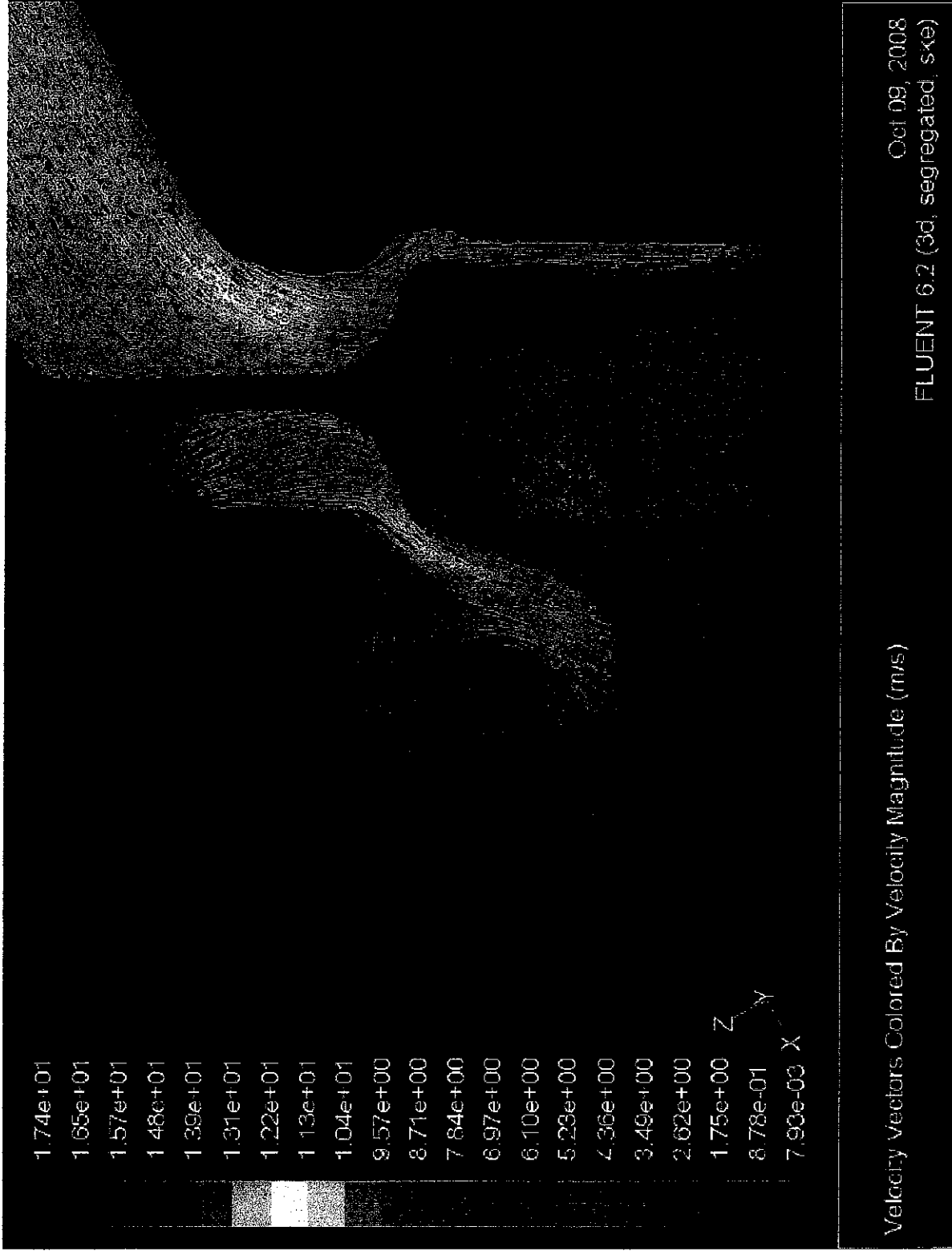
Appendix E: Tumble pattern from 3D simulation of 200mm length variation



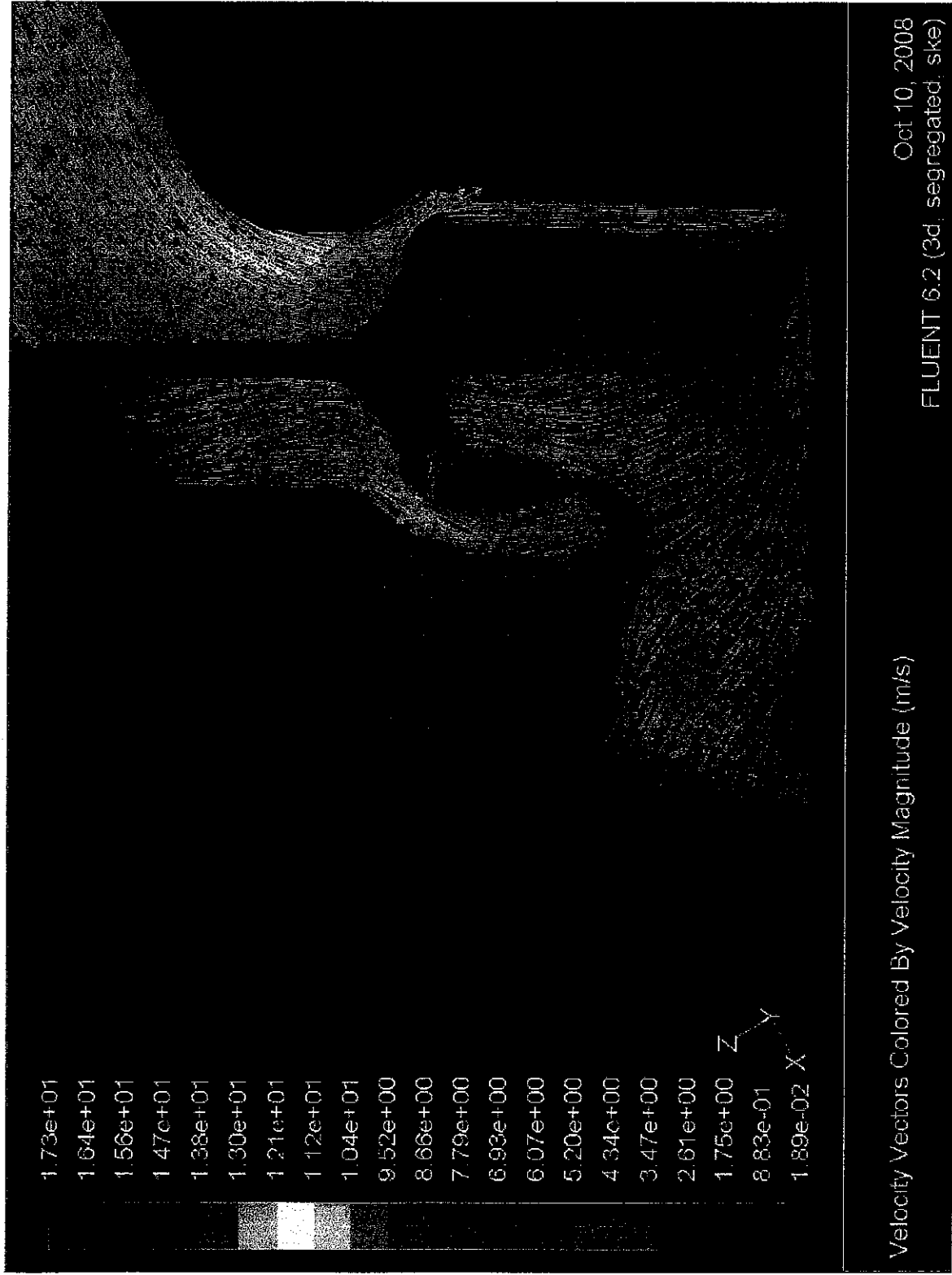
Appendix F: Tumble pattern from 3D simulation of 210mm length variation



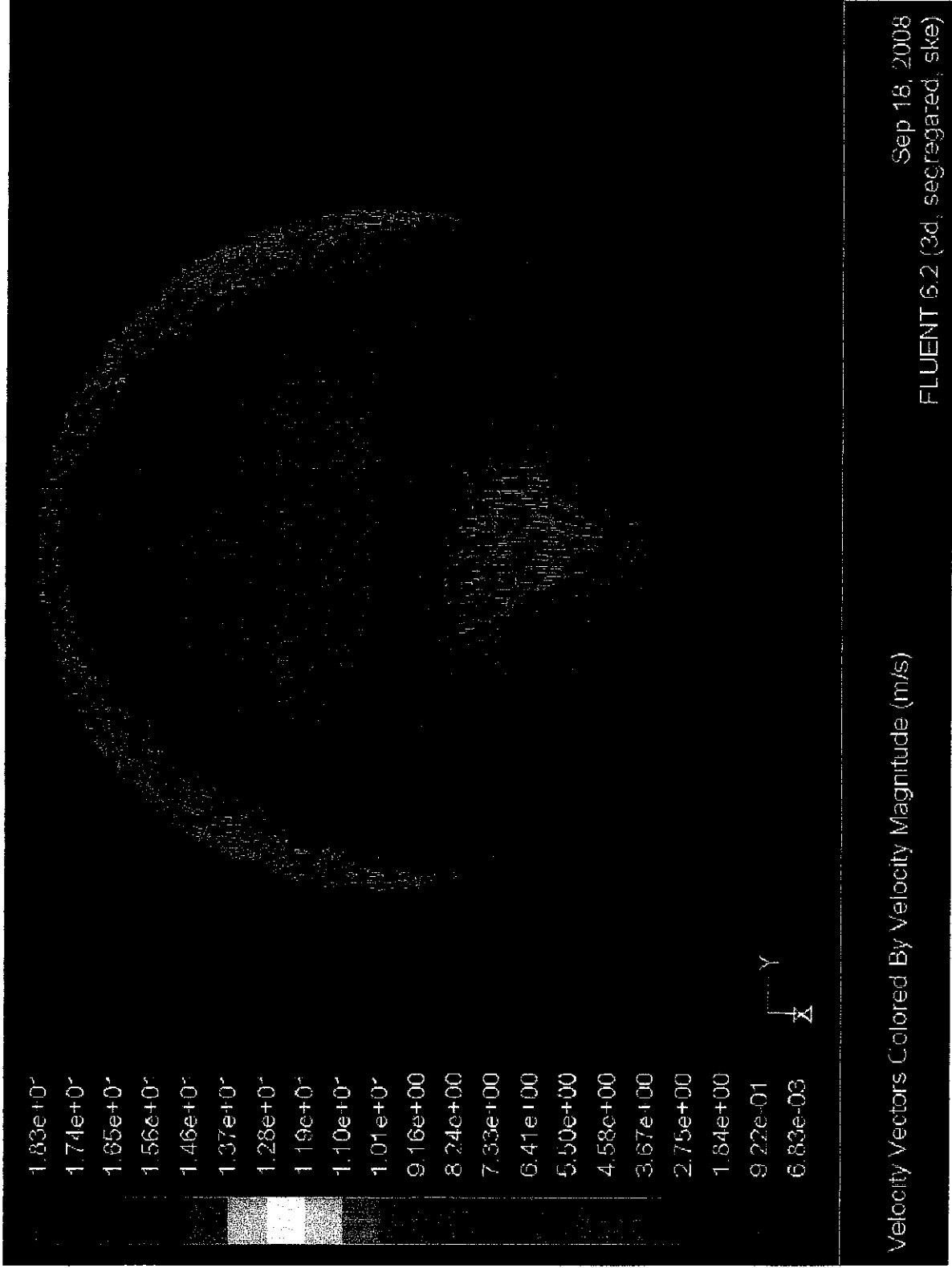
Appendix G: Tumble pattern from 3D simulation of 220mm length variation



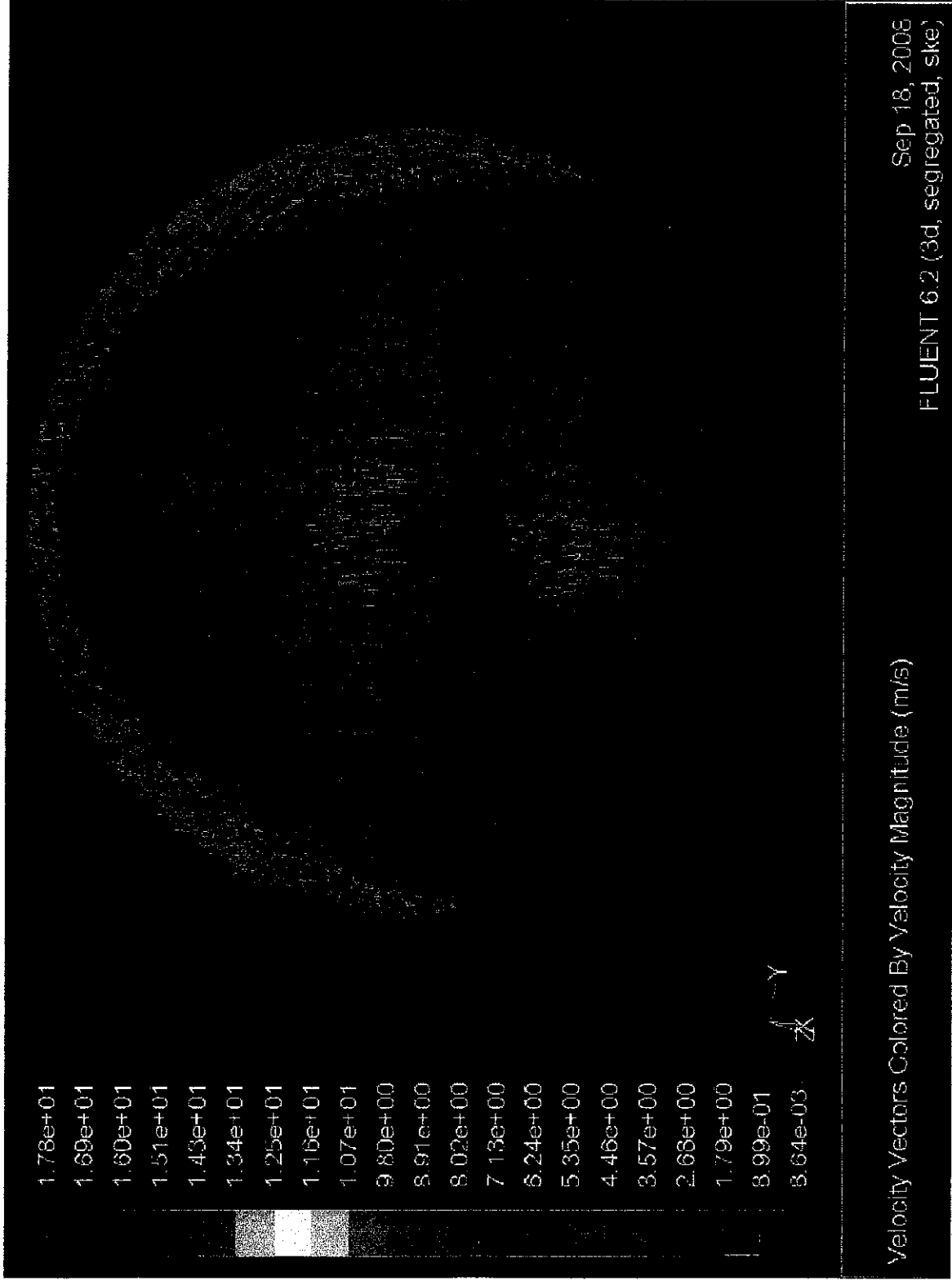
Appendix H: Tumble pattern from 3D simulation of 230mm length variation



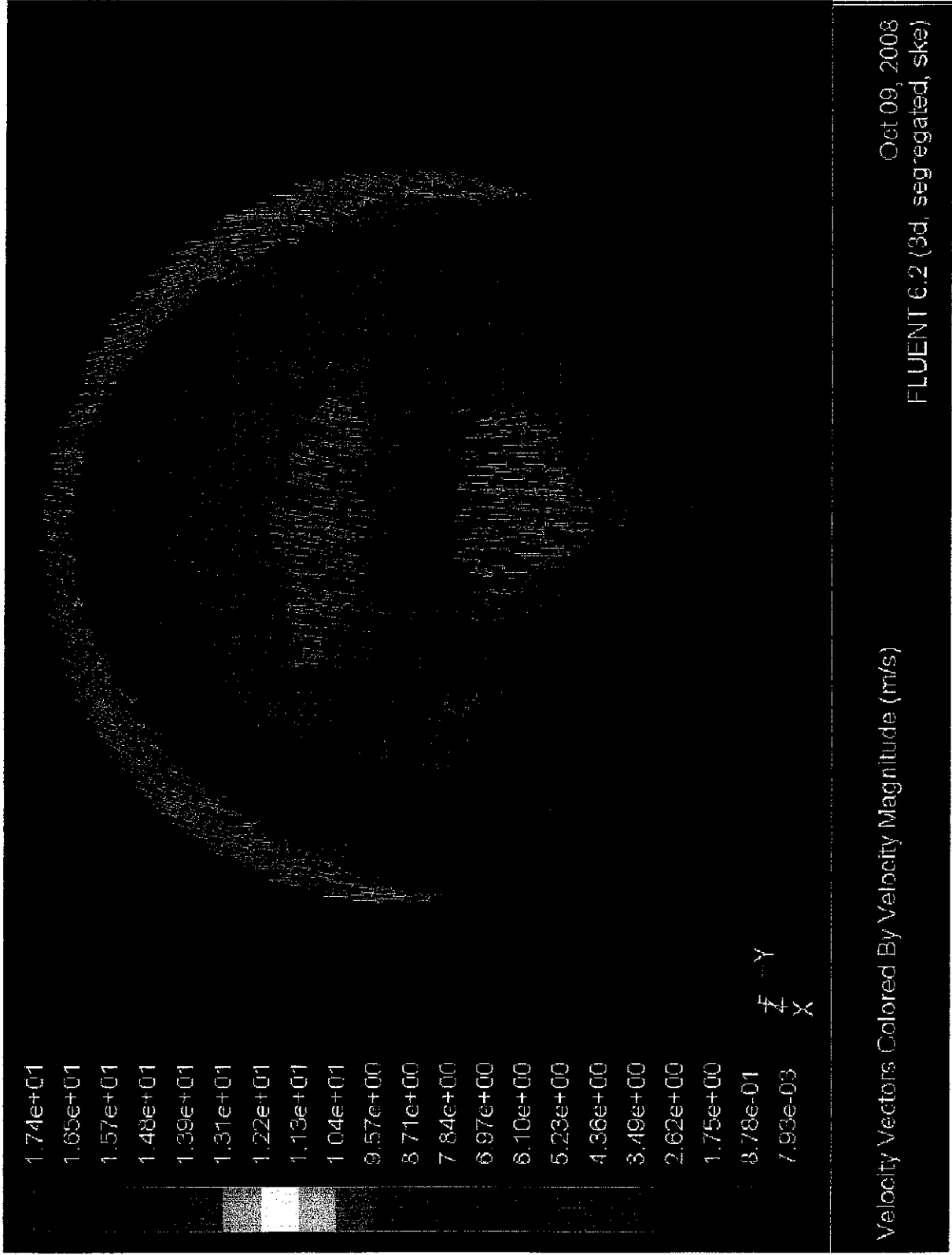
Appendix I: Swirl pattern from 3D simulation of 200mm length variation



Appendix J: Swirl pattern from 3D simulation of 210mm length variation



Appendix K: Swirl pattern from 3D simulation of 220mm length variation



Appendix L: Swirl pattern from 3D simulation of 230mm length variation

